1986

Optical characterization of lithium plasma produced by laser irradiation.

Hoselton, Bruce A.

NAVAL POSTGRADUATE SCHOOL
Monterey, California

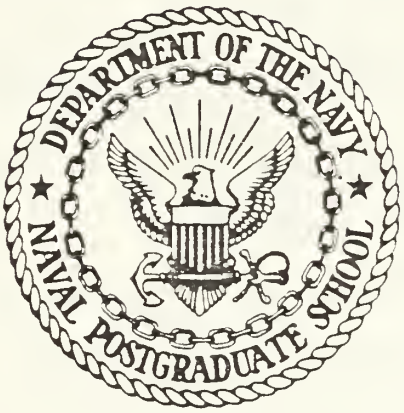

THESIS

OPTICAL CHARACTERIZATION OF LITHIUM
PLASMA
PRODUCED BY LASER IRRADIATION

by

Bruce A. Hoselton

December 1986

Thesis Advisor F.R. Schwirzke
Co-Advisor G.C. Tisone

Approved for public release; distribution is unlimited

SECURITY CLASSIFICATION OF THIS PAGE

REPORT DOCUMENTATION PAGE

1a REPORT SECURITY CLASSIFICATION UNCLASSIFIED	1b RESTRICTIVE MARKINGS
2a SECURITY CLASSIFICATION AUTHORITY	3 DISTRIBUTION/AVAILABILITY OF REPORT Approved for public release; distribution is unlimited.
2b DECLASSIFICATION/DOWNGRADING SCHEDULE	
4 PERFORMING ORGANIZATION REPORT NUMBER(S)	5 MONITORING ORGANIZATION REPORT NUMBER(S)
6a NAME OF PERFORMING ORGANIZATION Naval Postgraduate School 6b OFFICE SYMBOL (If applicable) 61	7a NAME OF MONITORING ORGANIZATION Naval Postgraduate School
6c ADDRESS (City, State, and ZIP Code) Monterey, California 93943-5000	7b ADDRESS (City, State, and ZIP Code) Monterey, California 93943-5000
8a NAME OF FUNDING/SPONSORING ORGANIZATION 8b OFFICE SYMBOL (If applicable)	9 PROCUREMENT INSTRUMENT IDENTIFICATION NUMBER
8c ADDRESS (City, State, and ZIP Code)	10 SOURCE OF FUNDING NUMBERS PROGRAM ELEMENT NO / PROJECT NO / TASK NO / WORK UNIT ACCESSION NO

11 TITLE (Include Security Classification)

OPTICAL CHARACTERIZATION OF LITHIUM PLASMA PRODUCED BY LASER IRRADIATION

12 PERSONAL AUTHOR(S)
Hoselton, Bruce A.

13a TYPE OF REPORT	13b TIME COVERED	14 DATE OF REPORT (Year, Month, Day)	15 PAGE COUNT
Master's Thesis	FROM _____ TO _____	1986 December	63

16 SUPPLEMENTARY NOTATION

17 COSATI CODES			18 SUBJECT TERMS (Continue on reverse if necessary and identify by block number)
FIELD	GROUP	SUB-GROUP	Laser produced plasmas, Unipolar arcing, LIBORS, ion source, Stark broadening

19 ABSTRACT (Continue on reverse if necessary and identify by block number)

Solid lithium deposited on stainless steel (SS) was irradiated by a CO_2 laser at 10.6 μm, and by a dye laser tuned to 666.4 nm and to the first resonance line of lithium, 670.8 nm. Type 316 SS surfaces were irradiated by a dye laser at 670.8 nm. Power densities ranged from <0.1-9.4 MW/cm^2. Optical information from the lithium plasma produced was evaluated using Stark broadening analysis to determine the plasma density, which varied from ~ 2×10^{16}/cm^3 to over 10^{17}/cm^3. Lithium and SS surfaces were observed by an SEM before and after irradiation, and evidence of unipolar arcing was found on both surface types.

20 DISTRIBUTION/AVAILABILITY OF ABSTRACT ☒ UNCLASSIFIED/UNLIMITED ☐ SAME AS RPT ☐ DTIC USERS	21 ABSTRACT SECURITY CLASSIFICATION UNCLASSIFIED
22a NAME OF RESPONSIBLE INDIVIDUAL F. Schwirzke	22b TELEPHONE (Include Area Code) (408) 646-2635 22c OFFICE SYMBOL 61Sw

DD FORM 1473, 84 MAR 83 APR edition may be used until exhausted
All other editions are obsolete

SECURITY CLASSIFICATION OF THIS PAGE

Approved for public release; distribution is unlimited.

Optical Characterization of Lithium Plasma Produced by Laser Irradiation

by

Bruce A. Hoselton
Lieutenant, United States Navy
B.S.M.E., University of Nebraska, 1979

Submitted in partial fulfillment of the
requirements for the degree of

MASTER OF SCIENCE IN PHYSICS

from the

NAVAL POSTGRADUATE SCHOOL
December 1986

ABSTRACT

Solid lithium deposited on stainless steel (SS) was irradiated by a CO_2 laser at 10.6 μm, and by a dye laser tuned to 666.4 nm and to the first resonance line of lithium, 670.8 nm. Type 316 SS surfaces were irradiated by a dye laser at 670.8 nm. Power densities ranged from <0.1-9.4 MW/cm^2. Optical information from the lithium plasma produced was evaluated using Stark broadening analysis to determine the plasma density, which varied from $\sim 2 \times 10^{16}$/cm^3 to over 10^{17}/cm^3. Lithium and SS surfaces were observed by an SEM before and after irradiation, and evidence of unipolar arcing was found on both surface types.

TABLE OF CONTENTS

LIST OF FIGURES

ACKNOWLEDGEMENTS

The author wishes to express his sincere appreciation for all who have assisted him in this endeavor. Specifically, at Sandia National Laboratory, Albuquerque, New Mexico, Doctors R.A. Gerber and G.C. Tisone were extremely helpful in aiding the author to gain the knowledge required for the accomplishment of the experiments conducted, and also allowed the author to utilize the Sandia National Laboratory facilities for the majority of the experimentation reported in this thesis. Also, the many hours of laboratory and technical assistance provided by Mike Hurst, Doctor J. Woodworth, Brian Clark, and Dora Wiemann which were critical in the accomplishment of experimental work, were greatly appreciated.

At the Naval Postgraduate School, the author expresses his appreciation for the assistance provided by his advisor, Doctor F. Schwirzke, and for the technical assistance provided by Tom Kellogg, George Jaksha, and Bob Sanders.

I. INTRODUCTION

The achievement of controlled thermonuclear fusion in the laboratory has been the goal of many scientists since the 1950's. Foremost in the reasons for this is the practically endless supply of energy, based on the abundance of deuterium fuel in ordinary water, and to the ability to mass produce tritium fuel. The DT (deuterium-tritium) fuel will undergo fusion and release large amounts of energy if held under extreme temperature and pressure for a sufficient amount of time. The primary methods of meeting the above criteria fall under the two major categories of magnetic confinement of a DT plasma, and inertial confinement of solid DT. One promising type of ICF (inertial confinement fusion) is the indirect implosion of a DT target by high velocity light ions in the Particle Beam Fusion Accelerator II (PBFA II), a light-ion accelerator presently undergoing testing at Sandia National Laboratory (SNLA). Presently, singly ionized lithium ions are the best choice, since they have a sufficiently small charge to mass ratio. This means that they can be effectively focused on the target and achieve sufficient kinetic energy for effective coupling to cause the desired target implosion [Ref. 1: p. 834].

Two of the potential ion sources that are likely to be tested first include a liquid lithium source which is electrohydrodynamically driven [Ref. 2], and a lithium-silver alloy that is rapidly heated to produce a lithium vapor, which is subsequently ionized by a laser [Ref. 3]. The latter process is quite complicated due to the multilayered construction of the anode that is required for the rapid ohmic heating of the lithium to a vapor [Ref. 1: p. 834]. However, it provides the ability to produce the desired lithium plasma in the laboratory instead of inside the accelerator environment, which is advantageous since this allows the relatively unhindered characterization of the plasma. Other methods which have been tested on prototype particle beam accelerators do not meet the established ion source requirements, ion density (n_i) $\geq 10^{17}$ per cubic centimeter (cc), and an ion layer of $\sim$ 1 millimeter (mm), for PBFA II [Ref. 4: pp. 1718-1721], and thus are not presently considered major contenders for future ion source studies.

This thesis will discuss the experimental results of a method to produce a sufficiently dense, thin lithium plasma which may satisfy the ion source requirements of

PBFA II. In order to efficiently accelerate lithium ions toward the DT target, the plasma is required to be present at the onset of a 30 Megavolt (MV) potential across an ion diode. In the experiments described here, a plasma was produced directly from solid lithium metal by a dye laser tuned to the first resonance line of lithium, at 670.8 nanometers (nm). It is theorized that two phenomona were combined in the production of this plasma; unipolar arcing, and laser ionization based on resonant saturation (LIBORS).

Unipolar arcing occurs when a laser-produced plasma is in direct contact with a conducting surface, and has been shown to be the predominant damage mechanism to that surface [Ref. 5: p. 10]. The damage occurs when an electric arc is established between the plasma and the surface, causing large numbers of particles to be ejected from the surface such that microscopic craters develop. Many neutral atoms are ionized in the laser heated plasma, resulting in an increasing plasma density which leads to more arcs, enhanced crater formation, and thus more material removed from the surface. The process continues as long as a sufficient laser power density is available. Considerable work has been accomplished to date on the study of unipolar arcing in various materials, such as on uncoated stainless steel (SS) and stainless steel coated with TiC (titanium carbide) [Ref. 6], and on semiconductor materials and metallic glasses [Ref. 7]. However, previous research on unipolar arcing was done in an attempt to prevent it from occuring due to the damage it caused on internal surfaces of magnetic confinement fusion devices [Ref. 8].

Once neutral lithium atoms are released from the surface, it is theorized in the present experiments that the LIBORS process occurs. An absorbed photon at the first resonant frequency of lithium excites the neutral atom. Subsequent collisions with hot electrons result in an ionization probability that is several orders of magnitude more [Ref. 9: p. 372] than that of a neutral atom irradiated and photoionized, after multiple photon-atom interactions, by a non-resonance laser. The result is a lithium plasma that is almost fully ionized at laser powers lower than those required for non-resonant laser plasma formation. The objective of this thesis was to determine the threshold energy density required for the onset of lithium plasma production, and to determine whether the added LIBORS process is able to produce a higher lithium plasma density from solid lithium than a non-resonant laser ionization process such as that caused during unipolar arcing. It will also determine whether unipolar arcing can be detected by detailed surface analysis under a scanning electron microscope.

This thesis will provide information under the following major headings: Background and Theory; Experimental Setup; Experimental Results; and Summary. The background and theory will describe the unipolar arc and LIBORS models as they apply to lithium. Equipment used and procedures followed for conducting the experiments are discussed. The results obtained and their comparison to theory are explained, and finally, recommendations for future experiments regarding equipment and target preparation are provided.

II. BACKGROUND AND THEORY

A. INTRODUCTION

Laser produced plasmas interact with surfaces in a variety of ways. The major contributors to damage, however, are classified by three processes; ion sputtering, thermal evaporation, and unipolar arcing. This chapter will outline the most recent extension of the unipolar arc model as presented by Olson [Ref. 10: pp. 14-32]. Olson's thesis includes a detailed treatment of the ion sputtering and thermal evaporation models, plus the historical development and detailed explanation of the currently accepted unipolar arc model.

The LIBORS process is then described, and the combination of the LIBORS process and unipolar arcing to produce a lithium plasma is discussed. It is assumed that the reader has a basic knowledge of plasma physics and laser-surface interactions, or has access to such material as the above referenced thesis for a more complete description and definition of terms used in this section.

B. OUTLINE OF UNIPOLAR ARCING MODEL

As a laser beam hits a surface, the energy which is not reflected heats the surface, causing desorption of the lighter surface contaminants, primarily gases and neutral atoms. If the photons have enough energy, for example 1.85 electron Volt (eV) photons from a dye laser tuned to a wavelength (λ) of 670.8 nm, some electrons may also be ejected from the surface. This is more likely, using the above example and assuming multiphoton interactions with the surface, if the surface is lithium, whose work function is 2.3 eV, than with iron, whose work function is 3.9 eV. If the surface is a conductor, such as lithium or SS, the tangential electric field from the laser electromagnetic wave at the surface is zero. Thus, an intensity maxima is established at a distance $\lambda/4$ from the surface, due to the superposition of the incident and reflected waves. Any electrons in the vicinity of $\lambda/4$, which is at 167.7 nm for the above wavelength, from the surface will oscillate with and gain energy from the electric field. Upon multiple collisions with neutral particles, many electrons will gain more thermal energy, establishing an electron temperature (T_e), such that subsequent collisions will ionize neutral atoms, and thus a weak plasma begins to form. At this point, if the laser is tuned to the first resonance line of lithium, the LIBORS process

can also occur and theoretically cause neutral lithium atoms to be ionized more readily, which is discussed in detail later.

Assuming a Maxwellian distribution of electron velocities, those electrons in the high energy tail of the distribution can quickly leave the vicinity of the much heavier ions, and many will reach the surface. This establishes what is referred to as a floating potential (V_f), defined by equation 2.1 as [Ref. 11: p. 3]:

$$V_f = (kT_e/2e) \ln (M_i/2\pi m_e) \qquad \text{(eqn 2.1)}$$

between the plasma and the surface, with the surface being more negative, where

k = Boltzmann's Constant

T_e = Electron Temperature

e = Electron Charge

M_i = Positive Ion Mass

and m_e = Electron Mass.

A plasma sheath has now been formed near the surface which electrostatically repels lower energy electrons back into the plasma, thereby maintaining quasi-neutrality in the plasma. The potential, V_f, causes an electric field (E_s) to be established across the plasma sheath, which can be approximated by $E_s \sim V_f/\lambda_D$ where λ_D is the Debye Length [Ref. 12: p. 780]. Because of E_s, ions can now be accelerated through the plasma sheath in equal numbers to the exiting high energy electrons and strike the surface, causing ion sputtering. This, combined with the continued laser desorption and, as the surface temperature increases, evaporation of more particles, leads to an increased density of neutrals being released into the plasma.

Electrons continue to gain energy in the $\lambda/4$ region from the surface and from further collisions with neutrals, so T_e increases which means $V_f \propto T_e$ also increases. From continued ionizations electron density (n_e) increases, causing $\lambda_D \propto n_e^{-1/2}$ to decrease. The above combined effects lead to a much increased value for E_s. Thus, with ion density (n_i) also increasing, more ions are accelerated to the surface to cause additional ion sputtering. Another factor leading to the increased release of neutrals is the heating of the surface from multiple ion-electron recombinations.

Even if plasma density reaches the critical density (n_c), which is about $2.5 \times 10^{21}/cm^3$ for the above wavelength, and laser energy is cut off from the surface, the free electrons in the plasma continue to gain energy as long as a sufficient laser power density is available to overcome losses. T_e thus continues to increase until the energy gain rate from the laser is matched by an energy loss rate due to ionizations and inelastic collisions. Therefore, V_f eventually reaches a maximum value in the plasma, which is about four volts per eV of the lithium plasma electron temperature, T_e.

As λ_D becomes $<< \lambda/4$, or on the order of 2×10^{-7} cm for the above λ, E_s approaches 10^7 volts/cm. Since the surface is not perfectly flat but contains many microscopic imperfections, those that protrude from the surface, called whiskers, serve to preferentially concentrate the electric field lines toward themselves. According to Halbritter [Ref. 13] this concentration of field lines can lead to an enhancement in E_s by a factor of 10-1000. This enhanced E_s "focuses" the ions to bombard the whisker, so that neutral particle density rapidly increases above the whisker, causing an increased n_i and n_e from ionizations, and thus λ_D will continue to decrease. In the region above the whisker, E_s quickly reaches $E_{arc} \sim V_c/\lambda_D \leq V_f/\lambda_D$, where V_c is called a cathode fall potential and refers to the potential that exists where an arc has been initiated. Thus the arc is initiated, probably by a phenomena known as enhanced field emission [Ref. 14].

Once the arc, which initially is comprised of electrons exiting the tip of the whisker and ions from the plasma bombarding the whisker, has begun, plasma density rapidly increases directly above the whisker. Therefore λ_D decreases more and E_{arc} continues to increase. Thus, the arc is a self-feeding mechanism as long as neutrals continue to be made available for ionization and collisions and electrons continue to gain the energy required for ionization of the neutrals. The continuation of the arc eventually leads to the formation of a crater where the whisker was. Due to the greatly increased plasma density above the arc crater, a radial electric field (E_r) is established from the resulting plasma pressure gradient. This provides for a reduced potential ring around the high density region [Ref. 15: pp. 10-11], which is depicted in the unipolar arc model shown in Figure 2.1 [Ref. 15: p. 11]. It is through this reduced potential area that electrons can return to the surface and complete the current loop. Since the surface acts as both cathode and anode, this entire process has been called unipolar arcing.

Eventually the plasma density increases enough that electrons begin to lose energy due to excessive inelastic collisions, so T_e and thus E_{arc} begin to decrease in the localized arc area. Also, as the plasma conforms to the surface of the crater and extends into it, the probability of high energy electrons reaching the increasing numbers of neutrals being ejected from the surface begins to decrease, and the subsequent decreased ionization rate further decreases E_{arc}. The combined result leads to the cessation of the arc, and the event is complete. The rim of the newly created arc crater may now protrude sufficiently to act as a new whisker, and if the necessary plasma conditions exist a new arc could be initiated.

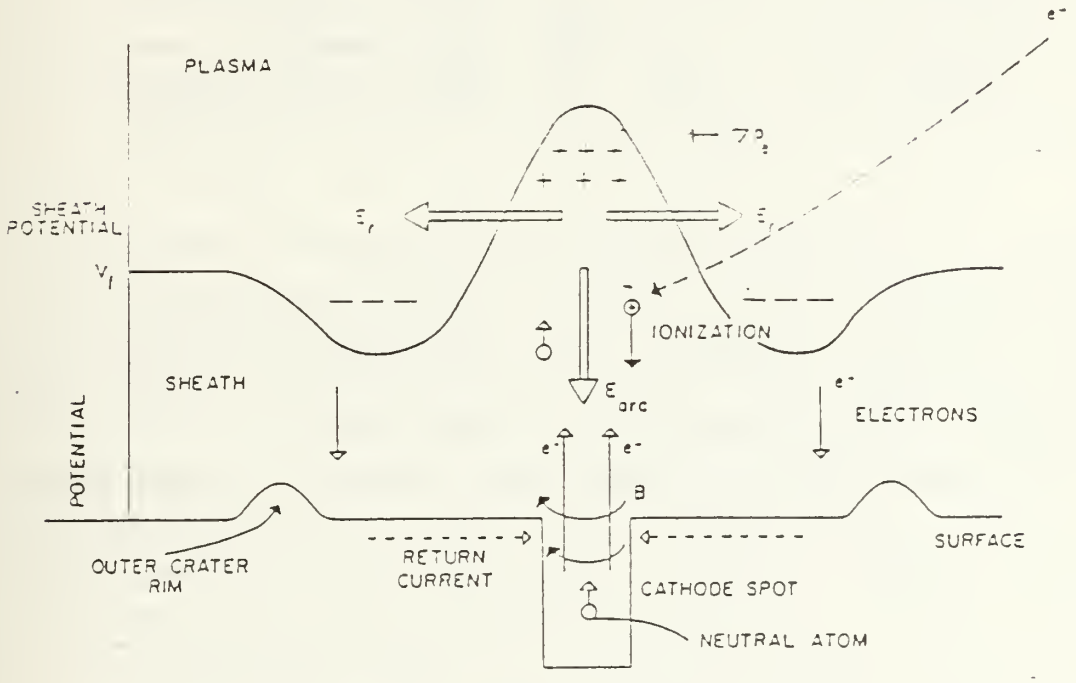

Figure 2.1 Unipolar Arc Model.

C. LIBORS MODEL

The direct photoionization of lithium is an inefficient process because the cross section for absorption is extremely low, at best about $2 \times 10^{-18}/cm^2$ for photon energies slightly above the ionization potential [Ref. 16]. In 1970, Measures [Ref. 17] suggested that the saturation of an atomic resonance transition of vapor by a laser should result in an efficient coupling of laser energy with the vapor. This would, he predicted,

substantially enhance the ionization of the vapor into a plasma. This was demonstrated on a lithium vapor in 1977 by McIlrath and Lucatorto [Ref. 18] using a 1 MW dye laser tuned to the first resonance line of lithium, at 670.8 nm. The experimental setup included a 15-cm-long lithium heat-pipe oven, and the vapor density was $\sim 6 \times 10^{15}/cm^3$. Based on densitometer traces taken at 200 ns intervals, it was reported that considerable ionization had taken place by 400 ns after laser initiation, and by 600 ns ionization was almost complete. Comparing similar work done with sodium (Na) vapor and by the process of elimination of various processes which lead to ionization, the paper narrowed the probable reasons for such an efficient and rapid ionization to one candidate, involving superelastically heated electrons.

Measures [Ref. 19: p. 2673], providing a detailed explanation of the above process, reasoned that because of an overpopulated resonance level caused by laser saturation of the resonance transition, any free electrons which interact by deexcitation or superelastic collisions with those excited atoms would experience a rapid increase in energy. He further proposed that, since a large excess population was being maintained in the resonance or excited state solely due to laser radiation, that there existed a pseudo-ground-state which effectively resulted in a much reduced ionization energy. Thus the rate of ionization should be enhanced greatly due to, in the former case, a much elevated electron temperature (T_e), and in the latter case due to excited atoms which would require less energy to become fully ionized.

The initiation of the Laser Ionization Based On Resonant Saturation (LIBORS) process requires some free electrons, which Measures proposed most likely come from three-photon ionization. Using the example of lithium and a laser wavelength of 670.8 nm, three photons at 1.85 eV each would provide 0.16 eV more than that required for lithium ionization. The newly freed electrons can undergo superelastic collisions with laser excited lithium atoms and quickly gain energy.

In a more detailed treatment, the four stages of the LIBORS process was proposed [Ref. 20: pp. 805-807] and is presented in Figure 2.2 [Ref. 20: p. 806]. As shown, the four stages are: laser saturation; seed electron creation period; intermediate ionization period; and ionization burnout. Laser saturation occurs within < 1 ns, with the result being that the ratio of the resonance state to ground state degeneracies is now the same ratio as resonance to ground state population densities. Thus, almost 3/4 of the original atoms in the ground state are now in the resonant or excited state. [Ref. 20: pp. 805-806]

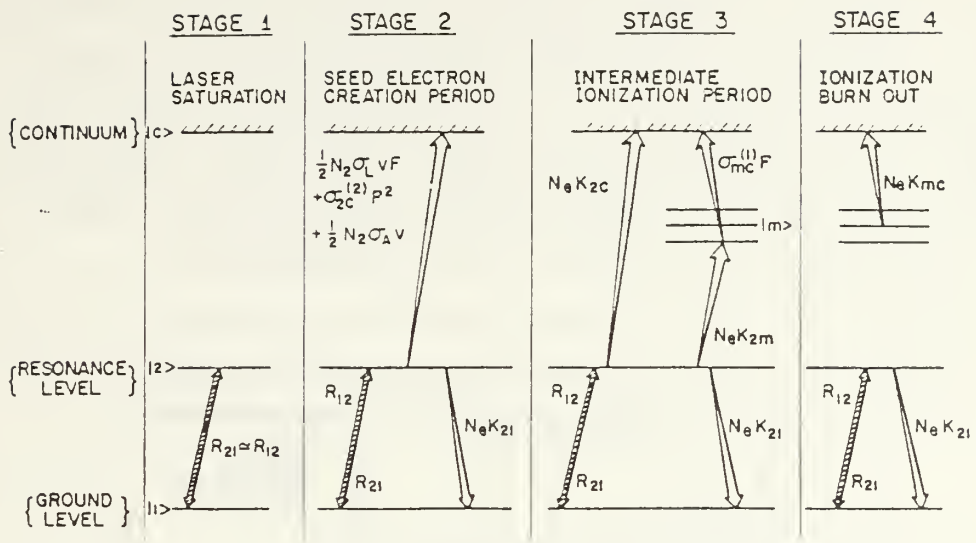

Figure 2.2 Four Stages of LIBORS.

The second stage, the creation of seed electrons, occurs primarily by three methods. The first is the two-photon ionization of the resonance level atom, which has already utilized one photon in order to be in the excited state. The product is an ion plus a free electron. The second method, called laser induced Penning ionization, occurs when two excited atoms interact together and with a photon to produce an ion, an electron, and a ground state atom. Thirdly, by associative ionization, two excited atoms interact to form a singly ionized dimer (molecule) plus an electron. In all three cases, the resulting particles have kinetic energy. The new free electrons quickly gain energy through "superelastic collision quenching of the laser sustained resonance-state population," as previously described. Thus, in the third stage, these energetic electrons can ionize resonance level atoms by direct collisions. At the same time, since many atoms experience "collisionally populated intermediate levels," which means that they are further excited to above the first resonance level, they can now be single photon ionized. The net result is an electron density which grows exponentially. [Ref. 20: p. 806]

Once a critical n_e is reached, the intermediate levels undergo unimpeded collisional ionizations, and a nearly complete ionization is reached in the excited

atomic species. This phenomena is referred to as ionization burnout. A graph of the increase in n_e vs time, for lithium vapor and a laser flux of 10^5 W/cm^2, is shown in Figure 2.3 [Ref. 20: p. 810], where stages two through four of the LIBORS model are depicted. It can be seen from the figure that the entire ionization process of a dense ($\sim 10^{16}$/cm^3) lithium vapor occurs in an extremely short amount of time using LIBORS. Using the LIBORS process is much more efficient because the resonant absorption cross section is several orders of magnitude larger at about 10^{-12}/cm^2 [Ref. 21] when compared to the value for ordinary photoionization.

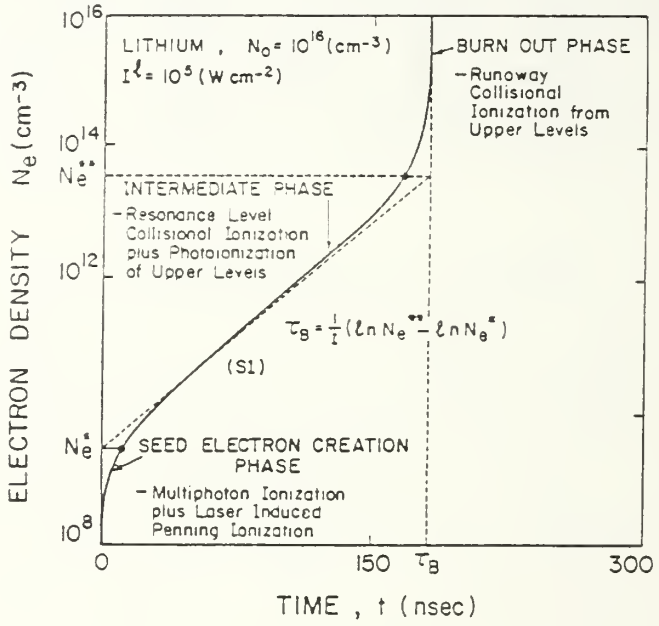

Figure 2.3 Electron Density versus Time for Lithium.

D. LIBORS AND UNIPOLAR ARCING COMBINED

Since the LIBORS process requires a vapor source, when a solid surface such as lithium is used the neutral atoms must be produced by direct vaporization from the application of heat, or by a process such as the unipolar arcing mechanism. The arcing process, although determined to be a destructive, non-uniform surface phenomena, will cause a rapid layer of neutral atoms and ions to be formed above the surface. Because of pressure and density gradients, the combined plasma and vapor should self-adjust to become more or less uniform over the surface, and the result should be a relatively

uniform density plasma layer, on a macroscopic scale, over the surface. A uniform plasma is a mandatory requirement for a suitable ion source in an ion diode.

Once a source of neutral lithium atoms is established, the LIBORS process can occur in the four staged sequence described above. Although the seed electrons will quickly gain energy from superelastic collisions, an additional energy source is available to those electrons at a distance of $\lambda/4$ from the surface due to the above described laser intensity maxima established at that point. Thus, the unipolar arcing and LIBORS processes should be complimentary in nature and provide a rapidly formed, dense lithium plasma. A limitation would possibly occur due to the rate at which neutral atoms could be released from the surface of the metal, and another limitation could occur when neutrals closer to the surface become shielded from the laser energy due to plasma cutoff.

The purpose of this thesis was to compare Li plasma densities produced by laser irradiation at both on- and off-resonance wavelengths, to test whether the LIBORS process combined with unipolar arcing would result in a higher density at lower power levels than with unipolar arcing alone. Another main objective was to determine the threshold laser power density required to produce a dense layer ($\sim 10^{17}/cm^3$) of lithium ions suitable for accelerator ion source requirements. It was with this in mind, and that the combined processes could provide a sufficiently dense plasma source of lithium ions for subsequent use in an ion accelerator, that the experiments in this thesis were conducted.

III. EXPERIMENT DESIGN

A. EQUIPMENT DESCRIPTION AND SETUP

The apparatus used for this experiment included a tuned dye laser, several laser diagnostics, an evacuated target chamber, and an optical multichannel analyzer (OMA) to gather plasma spectral information. A scanning electron microscope (SEM) was utilized for pre- and post-target irradiation surface study, to determine the undamaged and damaged characteristics of the lithium surface. The targets were type 316 stainless steel (SS) disks, onto which solid lithium had been deposited by various methods. Figure 3.1 depicts the laser and target chamber setup. The OMA equipment schematic is shown by Figure 3.2. Photographs were taken of the profile of target surfaces to record visual evidence of plasma formation and its extent.

1. Laser

A Candela SLL-625 Dye Laser System was used to provide the energy on target for plasma production. The majority of the data were gathered while the laser was tuned to an output wavelength of 670.8 nanometers (nm), which coincides with the first resonance line of lithium. Several shots were also taken at an off-resonance wavelength for comparison. Using sulforhodamine 640 dye, the laser had an effective tuneable wavelength range from 615 nm to 678 nm with peak efficiency centered at 640 nm, and in order to reach a suitable power level of a few megawatts (MW) per square cm at 670.8 nm, oxazine 720 dye was added and mixed with the sulforhodamine 640. The laser beam diameter was approximately 16 millimeters (mm).

The power supply to the laser flashlamp was charged to 25 kilovolts (kV). Although the laser output energy could be altered by changing the flashlamp voltage input, neutral density filters were used so the laser could be operated under known conditions. More detailed information on the laser system can be found in the instruction and installation manual [Ref. 22]. A helium-neon (He-Ne) laser was used for alignment and calibration.

It was discovered that the actual laser parameters, wavelength, power output, pulse width and pulse intensity varied from shot to shot. The factors that caused these variations were dye pump speed, the number of shots taken on and the age of the dye, dye temperature, time between successive shots, flashlamp output, and optical

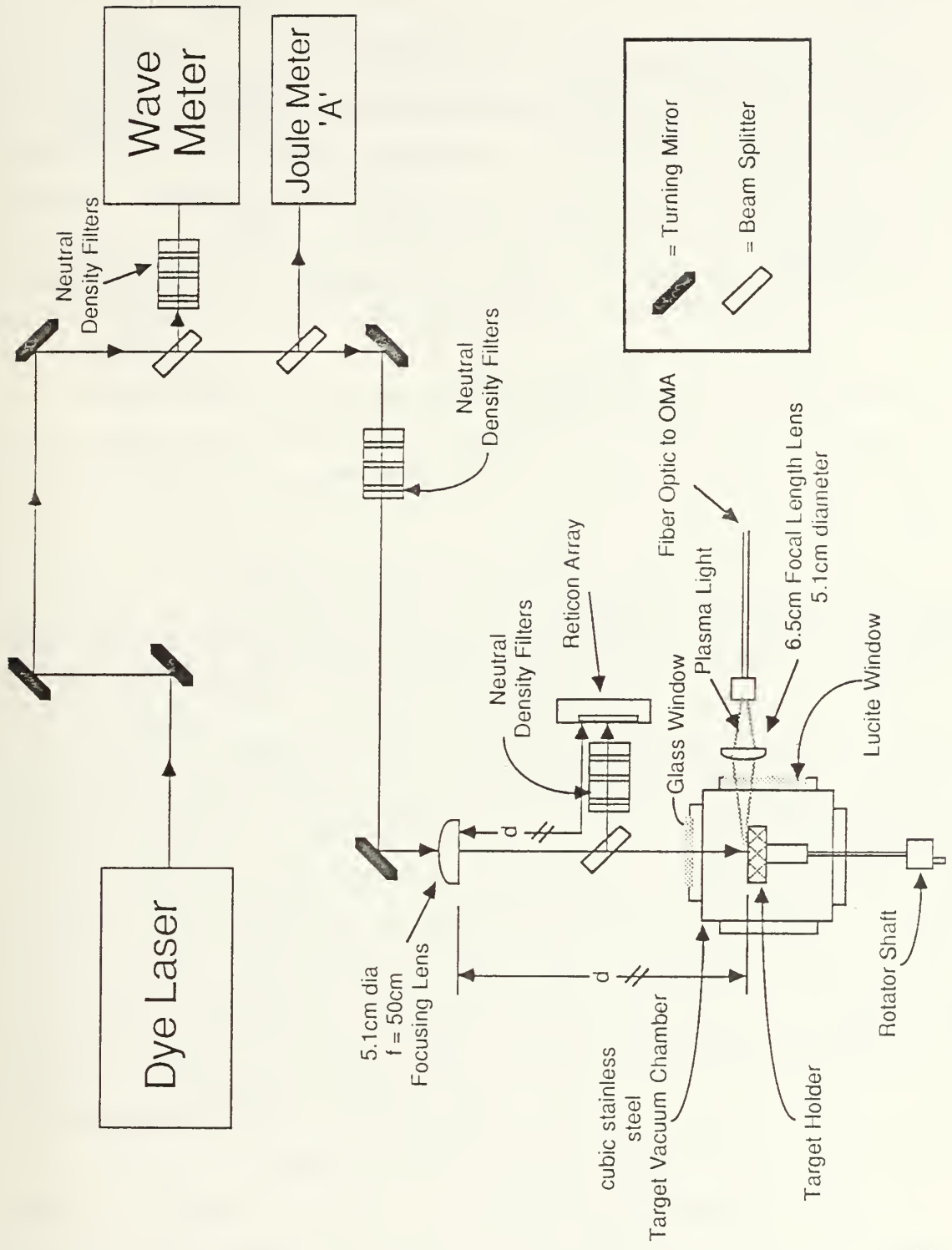

Figure 3.1 Laser, Diagnostics, and Target Chamber Setup.

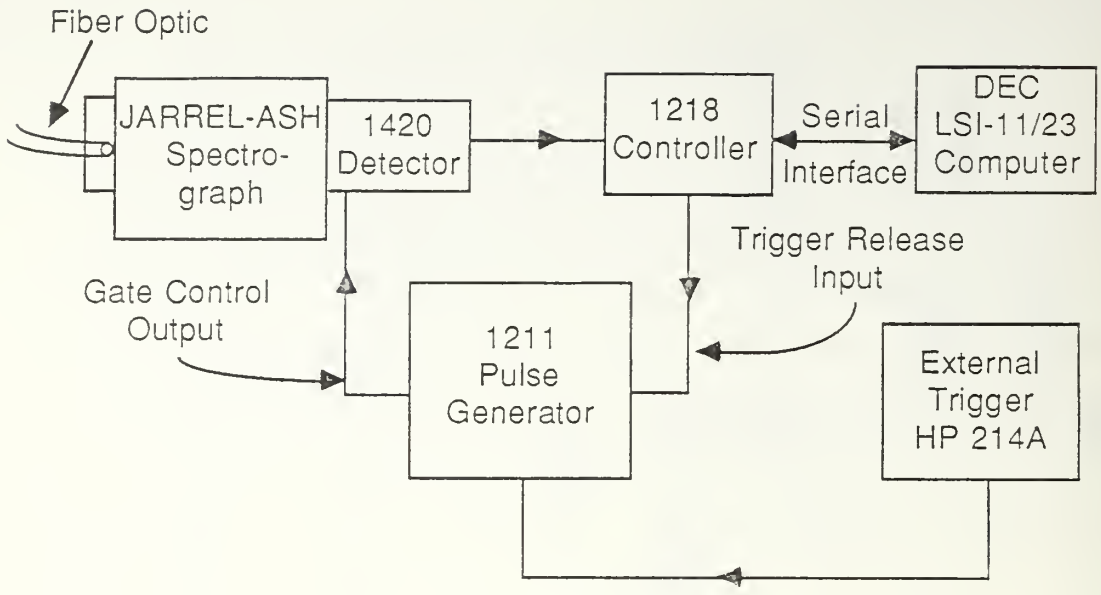

Figure 3.2 OMA System Schematic Diagram.

alignment variations due to temperature. The predominant factor for shot to shot variations was found to be time between successive shots, which affected the stability of the dye temperature. The predominant factor for long term power output degradation was the number of shots taken on a given dye mixture. A factor of three to five drop in power was experienced from the time a new dye mix was used until the approximate end of life of the dye. This was determined by low power output, poor beam quality, wide linewidth in nm, and a short pulse width. Therefore, the below described equipment setup was required to monitor the important shot to shot beam parameters. Additionally, pulse width was found to remain fairly constant for day to day operation and was monitored only before or after a sequence of shots used for data. The pulse width was detected by an ITT F-4018 type S-20 photodiode via a beam splitter, and displayed on an oscilloscope for analysis or recording by a camera. During the life cycle of the dye, the full width half maximum (FWHM) pulse width was found to vary from 900 ns for new dye to $\leq$ 500 ns for old dye.

2. **Laser Output Diagnostics**

a. Wavelength and Pulse Shape

Shot to shot wavelength data were provided by a Candela LS-1 Laser Spectrometer (wave meter), which used a He-Ne laser for reference. The wave meter was triggered by a Hewlett Packard (HP) model 214A pulse generator. The laser pulse reflected off a beam splitter was incident upon an array of photodiodes whose dimensions and distance apart were known. The reference and dye laser pulse shapes were displayed on an oscilloscope and were marked by two reference lines controlled from the wave meter. The difference, read directly from the wave meter, was used to calculate the actual wavelength to ± 0.01 nm.

b. Energy

Two Gentec Joulemeter ED-200 energy meters were used. Meter 'A' obtained energy from a beam splitter downstream of the wave meter beam splitter, and was used for shot to shot measurements. Meter 'B' was placed inside the opened target chamber with the targets removed, in order to record actual energy on target. Several shots were taken and ratios were obtained between the two meters to account for losses due to the focusing lens, an additional beam splitter, the chamber window, and numerous neutral density filters used to reduce power on target. The meters were calibrated to an accuracy of 10 percent (%).

c. Spot size

Focused laser power was incident upon a Candela Model RSX-1 reticon array via a beam splitter and several neutral density filters for protection. The distance from the 50 centimeter (cm) focal length lens to the array was the same as the distance to the targets, and spot size information was found by displaying the pulse on an oscilloscope. Reference markers were provided by a Candela RD-2 Reticon Digitizer which, after manual adjustment upon each shot, gave a direct readout of the number of reticon elements illuminated at the FWHM spot size. The distance between each element was 25 μm, and thus the number of elements illuminated was multiplied times 25×10^{-4} to obtain the spot diameter in cm.

3. **Target Chamber**

The target chamber was a 15.2 cm cube of SS, with a glass window on the optical axis and a lucite window at 90° off axis. The laser energy was incident normal upon the vertical aluminum target holder, which was 7.5 cm in diameter and contained six targets, each 12.7 mm in diameter. The laser spot was centered on the targets,

which were sequentially moved into position by the externally manipulated 6.35 mm shaft onto which the target holder was fitted. A Sargent-Welch Model 1402 roughing pump was used both alone to maintain a 4 to 5×10^{-4} torr vacuum for storage and protection of the lithium samples, and in series with a Varian Model VHS-4 diffusion pump to maintain vacuum at 1 to 4×10^{-6} torr for experimental target shots. For additional target protection, a compressed-argon filled gas bottle was connected to the vacuum chamber for backfill into the chamber before and during all times that the lithium targets were transferred into or out of the chamber. The vacuum system table provided a convenient surface upon which was attached a 50 cm focal-length lens, a beam splitter, a filter holder and reticon array unit, as well as a 6.5 cm focal-length lens and a fiber optic cable and holder for plasma light transmission.

4. **Optical Multichannel Analyzer System**

An EG&G Princeton Applied Research OMA-2 detector system was utilized, which consisted of several different types of equipment, described below, necessary to gather and analyze plasma light from the lithium target via a 4-m-long fiber optic cable. The equipment was manufactured by EG&G unless otherwise noted. See Figure 3.2. The fiber optic cable was placed in position at 90° off axis. A 5.08-cm-diameter, 6.5-cm-focal-length lens was positioned about 13 cm from the target center to gather as much plasma light as possible, and the fiber optic was placed at about 12 cm from the lens to obtain the most intense, focused plasma image at the optic cable end. An equipment description is provided below, but for more detailed information see the EG&G technical note No. 181 [Ref. 23], or the respective equipment operating and service manuals [Refs. 24,25].

a. Spectrometer

The fiber optic outlet was connected via a centering notch to a Jarrell-Ash "1-meter" spectrometer, which provided a grating to restrict the actual spread of wavelengths transmitted to the OMA to a bandwidth of 13.58 nm. The spectrometer was adjustible to permit the peak of the desired wavelength profile to be centered on the detector reticon array for analysis.

b. Detector

Light from the spectrometer was channeled into a model 1420 solid state intensified diode array detector via a gate, which could be timed to open for a specific interval or kept open for continous wavelength operation. This detector used a 730 channel proximity focused micro-channel plate intensifier, which had the capability of

being gated open for as short as a five ns interval without signal degradation. Channel sensitivity was factory preset at one count per photoelectron, and the built in amplifier was capable of passing 700 channels of information. Electrical power was supplied by a model 1218 solid state detector controller.

c. Pulse Generator

Gate control for the detector was provided by a model 1211 high voltage pulse generator, which had the capability of triggering the OMA gate to be open for as short as 10 ns or for as long as 999 μs. The generator could also delay the gate open start time for 100 ns up to 999 ms in order to allow the detector to look at a distinct time interval during the laser-target interaction-plasma production cycle. For the experiments reported in this thesis, the delay time was set to 100 ns and the gate was set to be open for 900 μs. Trigger release for the model 1211 came directly from the model 1218 detector controller, which received its triggering ultimately from the HP model 214A pulse generator, which also provided the trigger for the wave meter.

Therefore, the sequence of events that occurred when the detector controller was put in a ready status by a computer, was that the trigger button on the HP model 214A pulse generator was depressed, sending a signal to the model 1211 pulse generator and the wave meter at the same time. The model 1211 would then send a signal to the laser, which would produce a pulse at the lithium target, causing a short burst of plasma. The model 1211, preset to wait a certain amount of time, then sent a trigger to open the model 1420 detector gate just before the plasma light had travelled through the fiber optic and the spectrometer to reach the detector. The detector amplified and transmitted the plasma spectral signal to the model 1218 detector controller, which passed the channel by channel digitized information to the computer for edited numerical screen display.

d. Computer control and data storage

A Digital Equipment LSI 11 microprocessor and associated software provided the control signal to the model 1218 detector controller, in order to enable the model 1211 pulse generator to fire the laser and operate the detector gate mechanism. The computer would then receive the digitized plasma information from the detector controller, display certain parameters such as maximum and minimum relative intensity on the screen, and await further instructions, such as to save the information to disk, prepare for another shot, or other operations. A graphics program allowed the information to be displayed graphically for 700 channels, plotted horizontally, versus

relative intensity plotted vertically. Polaroid photographs were taken of the plotted CRT displays for subsequent plasma line broadening analysis.

5. Scanning Electron Microscope

A Hitachi S-450 scanning electron microscope (SEM) was used at Sandia National Laboratory to characterize and photograph the lithium target surfaces before and after irradiation with the laser. The SEM was capable of magnifications from 20X to 200,000X with a resolution of 6.0 nm. A hair-pin tungsten filament was used, and the system was capable of maintaining a vacuum of 5×10^{-6} torr. The system had no provision for any inert gas backfill, so lithium samples were exposed to air during all the transfer operations.

An additional SEM was used at the Naval Postgraduate School (NPS) for target studies. It was a Cambridge Stereoscan 200, with magnification ranges of 30X to 300,000X, a vacuum capability of 7×10^{-7} torr, and it used a hairpin tungsten filament. Additionally, a resolution of 7.0 nm was obtainable, and the system had a nitrogen gas backfill capability, which allowed much better protection of the lithium samples at ambient temperatures.

6. Lithium Handling Equipment

Lithium target preparation and handling was done in a Dry-Lab Glove Box, which included a Dri-Train M040-1 unit that maintained a positive atmosphere of 0″ to 1″(H_2O) of argon gas, and maintained very low oxygen, ≤ 1.0 parts per million(ppm), and water vapor, ≤ 0.5 ppm. Inside the glove box was a SYBRON/Thermolyne 1400 furnace, capable of over 1000°C, and various tools for the preparation and handling of lithium and lithium coated SS targets, such as needle nose pliers, scissors, a knife, SS scrapers, a ruler, allen wrenches, and more.

Anything entering the glove box had to pass through a sealed transfer chamber, which was first evacuated to < 150 torr vacuum. For added protection, the transfer chamber was normally kept under a vacuum to reduce the possibility of air or water vapor getting into the glove box. The transfer chamber was then backfilled with argon to equalize pressure with the glove box, and the equipment or parts being transferred could then be moved into the glove box. Anything exiting the glove box went through the same transfer chamber, but unless the chamber had been opened to atmosphere the evacuation was not done.

B. PROCEDURE

1. Target Preparation and Handling

Target substrates were all 12.7 mm diameter by 6.35 mm high type 316 stainless steel disks. The reason for this material selection was due to its acceptance for suitable liquid lithium containment at temperatures up to 500°C [Ref. 26: pp. 22-24]. However, in retrospect, a better material selection may have been niobium, tantalum, or molybdenum [Ref. 27], since the disks were kept at above 600°C and in contact with liquid lithium for as long as one hour during the target production process. The disks were polished on one of the flat surfaces by standard metallographic polishing techniques. The final polish solution was a 0.5 μm AlO_2 slurry, which yielded a mirror-like finish on each disk. This was done to provide a smooth, flat surface onto which a thin lithium foil of the order of several microns could be adhered. However, a suitable medium was not available that would adhere the disk to the thin lithium foil, maintain a flat, smooth surface, and also not react with the lithium, which proved to be a very difficult metal with which to work. Instead, for initial experiments, 5.08 cm × 381 μm thick lithium foil was cut into 7.9 mm wide strips by a pair of scissors, since lithium is softer than lead [Ref. 28].

Prior to being transferred into the argon filled glove box, the disks were ultrasonically cleaned in methanol for > 10 minutes, after which rubber gloves were used to handle them. The disks were placed on a 7.6 cm × 7.6 cm × 2.4 mm SS plate for handling, and into the furnace at 500°C. After being heated for one hour, the disks were removed from the furnace, and several attempts were made to melt the lithium foil onto the disks with no success. After the disks had been heated to 650°C, the lithium would melt onto the surface of the disks and immediately ball up, like mercury, instead of wetting the entire surface. The resulting acceptible procedure was to place the disks in the furnace which was heated to between 650°C and 700°C for a minimum of ½ hour, before melting the lithium pieces onto the disks.

Once the lithium had melted and balled up on the surface, the disks were placed back into the furnace for about five minutes, and then removed. At this point the lithium had usually wet the entire polished surface with a slight meniscus, which was mirror shiny like liquid mercury. If the entire surface was not covered, a scraper was used to spread the lithium over the remaining surface. The foil strips were cut to 7.9 × 14.3mm; less than this would result in difficulty in covering the entire surface, and more would result in an excessively rounded meniscus with an inadequate surface flatness.

Unfortunately, the shiny appearance would be replaced within a few minutes by a dull, cloudy film over the lithium surface. Apparantly, contaminants existing in the lithium foil, or reaction products between lithium and the SS disks, water vapor, or nitrogen, or any combination of the above, were precipitating onto the surface. This resulted in a noticable layer of residue on the surface and in white flakes, probably lithium hydroxide, at the lithium-SS boundary. A stainless steel scraper was used with limited success to scrape these contaminants off of the surface. This would usually result in the breaking up of the remaining film into several small particles, which would evenly disperse over the surface. As the lithium cooled down, it eventually became tacky and the scraper would either stick to it or remove excessive amounts of lithium metal. Thus the targets always required reheating at above 650°C for at least five to six more minutes.

The surfaces would always come out mirror shiny, but the same phenomena of clouding and film formation would occur, regardless of how many times the scraping and reheating procedure was done. In most cases, two cycles of scraping and reheating were the optimum for reducing surface contamination, with the surfaces being allowed to cool untouched after the final reheat. In one instance, using foil from the end of the roll, four scraping and reheating cycles still did not produce satisfactory samples. Even in a controlled atmosphere such as the glove box, exposed lithium deteriorates due to its extremely reactive nature. Other possible sources of contamination could be from the handling of lithium by steel scissors, the knife, scrapers, needle nose pliers, rubber gloves, paper napkins on which the foil was laid, the steel glove box chamber bottom, and inadvertant contact with glass, plastic, and other materials.

Significantly improved targets were prepared using lithium from 20.3 × 2.5 cm diameter bars, from which were sliced 2.4 mm thick disks of very pure lithium. The subsequent optimum sized pieces of lithium were about 2.4 × 2.4 × 9.5 mm. Using the bar lithium resulted in far superior surfaces with regard to low amounts of contaminants and final appearance. After two scraping and reheating sequences of the new targets the surface appeared much like the actual metal obtained from the protected inner material of the bar. Other work conducted while producing lithium coated structures at Sandia National Laboratory resulted in the same significant improvement in the reduction of contaminants when the lithium bars were used instead of the foil [Ref. 29].

To complete the target production cycle, at the end of the final reheat, the targets were removed from the furnace, taken off the hot 7.6×7.6 cm transfer plate and placed on the cool (ambient) chamber bottom for rapid cooling. Before being transferred into the glove box, the aluminum target holder assembly and brass set screws were ultrasonically cleaned for > 10 minutes in acetone, and then were handled only by rubber gloves or clean paper cloths. Once cold, the targets were placed in the six slots of the target holder, and set screws were used to hold the targets securely. When transferred from the argon glove box, an argon filled, sealed dessicator jar was used. This provided sufficient short term protection until the targets were placed in the SEM, during which they were exposed to air for up to two to three minutes during evacuation of the SEM, or in the laser target chamber, when exposure to air was reduced to several seconds.

When irradiation by laser and surface study was complete, or when the targets were so corroded that they were no longer useful, the lithium was cleaned off the SS disks by dropping them into a large beaker of water. Due to the rapid reaction with water which produced hydrogen, this was done in a well ventilated hood. Within minutes, the lithium was gone, and the disks were rinsed off by squirting them with methanol. Then to repolish the surfaces and clean the disks more completely, each disk was polished using a polish wheel and 1.0 μm diamond compound. Each surface would easily polish to a mirror luster, and thus each disk was able to be re-used several times. As before, prior to being transferred back into the glove box, the disks were ultrasonically cleaned for ≥ 10 minutes in methanol. Additionally, if the target holders became contaminated, they were also ultrasonically cleaned in acetone, as previously described, prior to re-use.

2. Laser Plasma Production

The production of lithium plasma was done in three different types of experiments. At first, when the OMA plasma analysis equipment was not available, several on-resonance laser shots were conducted on samples made from lithium foil, and also on polished type 316 SS surfaces. The samples were observed by an SEM for evidence of unipolar arcing and melting. After the OMA equipment was set up, samples produced both from foil strips and from pieces of pure lithium bar were irradiated. The dye laser was tuned to 670.8 nm on all targets. It was then changed to an off-resonance wavelength of 666.4 nm for a series of shots on one of the previously on-resonance irradiated targets, for plasma density comparison. Finally, a CO_2 laser,

with a wavelength of 10.6 μm and a pulse width of 4.55 μs, was used at the Naval Postgraduate School (NPS) to irradiate lithium targets produced by bar lithium. The surfaces were observed by the NPS SEM for visual evidence of unipolar arcing.

The experimental procedure was nearly identical in all three cases. The targets were removed from an argon filled, sealed glass jar and exposed to air for ≤ 10 sec while transferring to the vacuum chamber at SNLA with its argon backfill capability, or for 10 to 30 sec while transferring to the vacuum chamber with nitrogen backfill at NPS. The difference in exposure times was due to the ease of access and ability to close the system up faster in the former case. After reaching a vacuum of $\leq 4 \times 10^{-6}$ torr, the lasers were prepared for use. Several shots were always taken on the dye laser before target irradiation, in order to fine tune the wavelength, optimize pulse shape uniformity, and stabilize the temperatures of the dye and the optics. In the latter case, an interval of 20 to 25 sec between shots resulted in the best repeatability of energy output, wavelength, and beam quality and uniformity. Unfortunately, when taking the actual data, this interval was often exceeded, which mandated the shot to shot monitoring of all important pulse parameters. This was unnecessary for shots taken with the CO_2 laser, where only energy output was monitored on a shot to shot basis. Upon completion of all shots, the vacuum chamber was backfilled with its respective gas, and the target holders were placed and sealed in glass jars, which were prefilled with the same applicable gas. The targets could then be transferred to an SEM or stored for future use or disposal. The different experimental procedures are detailed below, and the results are discussed in the next chapter.

a. Experiment-Type 1

These experiments, conducted on targets made from lithium foil, were done to determine whether unipolar arcing could be detected on the target surfaces. A distinct, violet colored flash of light, which probably coincided with the 460.3 nm line of lithium, was evident whenever plasma was produced. When an insufficient laser power density was used, no light was detected. Power density on target was controlled by moving the 50 cm focal-length lens linearly toward or away from the target, keeping the distance to the target at a range of 40 to 50 cm away, thereby causing the irradiated area to increase or decrease. Neutral density filters were not used, and spot size measurements were obtained only from spots burned onto exposed polaroid paper which was secured to a target holder in the vacuum chamber. Several shots were taken in order to calculate an average spot size for each distance that was used on actual

targets. Also, several power meter comparison shots were taken, as described earlier, so that shot to shot pulse energy on target could be calculated. Finally, a pulse width measurement was obtained in order to convert energy density to power density.

Several shots were also taken on unused, polished stainless steel disks to obtain visual evidence of unipolar arcing, and to obtain power density information. Visual evidence of plasma production was simply the observation of white light being emitted from the target being irradiated.

b. Experiment-Type 2

The operation of the OMA system was described earlier in this chapter. Three different element hollow cathode tubes, lithium (Li), zinc (Zn), and mercury (Hg), were positioned, one at a time, to illuminate the end of the fiber optic near the target chamber. This was done to obtain information about the correction factor required between the actual line spectrum being observed and the spectrometer digital readout in nm. The correction requirement was introduced at the time of the initial alignment and calibration of the spectrometer, and was found to vary slightly over the range of interest, from 671.7 nm to 434.8 nm. For example, at the Hg 546.1 nm line, the correction was $\Delta = -51.9$ nm, and thus the spectrometer was manually set to 546.1-51.9 = 494.2 nm, which caused the Hg 546.1 peak to be centered in the oscilloscope display. However, at the Hg 435.8 nm line, the correction was $\Delta = -53.4$ nm. By interpolation, the desired Li 460.3 nm plasma line was calculated to be centered at the spectrometer setting of 407.2, and this proved to be correct. The above calculations were necessary due to the short time interval the Li 460.3 line was available to the OMA, which was operating in the gated mode of detection. The actual pulse was displayed on the CRT for only about 0.1 s.

To check the accuracy of the laser wave meter, the lithium hollow cathode tube was used to record the three lines, 671.7 nm, 670.8 nm, and 667.8 nm. A few laser pulses at 670.8 nm confirmed that the wave meter and OMA detector were recording the same wavelength. Near the Li 460.3 line, a Zn tube was used to examine the Zn 481.053 nm and 468.014 nm lines. These were recorded on the computer, and since they were almost 700 channels apart on the computer CRT, they were used to determine the number of nm per channel. The computer could plot any range of channels desired, and thus the above Zn lines were expanded and looked at closely, and the result was a ratio of 0.0194 nm/channel. At 0.0194 nm per channel, for a 700 channel plot, the CRT can display wavelength information obtained over a range of 13.65 nm.

The nm/channel information was important for the calculation of plasma density. A phenomena known as Stark broadening [Ref. 30: p. 63] is a type of broadening of spectral lines in dense plasmas. The broadening occurs due to electric fields produced by the motion and interactions of electrons and ions in a plasma, which for dense plasmas completely dominates any natural or Doppler broadening. Because the ions are much heavier than the electrons and thus move much more slowly, the acceptable broadening theory ignores ion motion, and instead relies on electron broadening calculations that are based on an electron impact approximation [Ref. 30: p. 72]. From table 4-5 of [Ref. 30: pp. 454-455] the calculations of electron impact half width half maximum (HWHM) in nm, for various electron temperatures in °K, were obtained. For the Li 460.3 nm line, assuming T_e was 10,000°K (or slightly less than 1 eV) the HWHM value was 0.149 nm for an equivalent electron density of $10^{16}/cm^3$. The maximum error in this value was 16.8% if T_e ranged from 5000°K to 20,000°K, which is well in the temperature range predicted by the LIBORS model [Ref. 20: p. 511].

To convert to a FWHM value, the HWHM number was doubled to become 0.298 nm. Thus, the FWHM value in nm, obtained from a computer generated plot of the broadened Li 460.3 plasma line, was multiplied by the ratio of $10^{16}/0.298$ to obtain the desired plasma density per cc. An assumption was made that only singly ionized Li ions were produced, which was reasonable based on the fact that the second ionization potential of Li is 75.6 eV, or more than one order of magnitude higher than the first ionization potential at 5.4 eV [Ref. 31: p. E-68]. Therefore, it can be assumed that the Li plasma density will be equivalent to the value obtained for electron density calculations. However, based on data collected from plasma production experiments, it was reported that the ratio of actual measured density to the predicted Stark density was 0.71 for the Li 460.3 nm plasma line [Ref. 32: pp. 239-240]. Thus all values of plasma density reported in this thesis and incorporated into any figures will have been multiplied by 0.71 in order to more closely approximate actual values.

Prior to collecting plasma data, several measurements were taken in order to conduct laser power density calculations. Average values of power meter ratios were obtained for unattenuated and attenuated laser pulses. Pulse width measurements were also obtained, and the reticon array was aligned to ensure the full laser spot diameter was being measured. Additionally, a "zero" shot was recorded on the computer by

disabling the laser and triggering the OMA detector. Therefore, ambient light and other noise near the fiber optic ends were recorded and subsequently subtracted from the desired plasma data, all of which was stored in computer data files on an eight inch floppy disk. Finally, two cleaning shots, to remove moisture and surface contaminants, were done on each target at a distance of 40 cm from the 50 cm focal-length lens. All data reported were taken on targets placed at a distance of 45 cm from the focusing lens.

The procedure for data collection on a set of six Li targets began by enabling the OMA system from the computer. Upon triggering the HP 214A pulse generator, which triggered the laser and the OMA detector as described previously in the equipment section, optical data from the irradiated Li target were automatically recorded by the computer. The data had to be saved to a disk, as the next set of data would be recorded over it, causing the old data to be lost. For each pulse, the 'A' energy meter reading and the reticon array reading were recorded. A log was maintained to record the above values and also the target number, the shot number on the target, the neutral density filter used, and the file name under which the plasma data were stored. The wave meter was checked after about every fifth shot to ensure that wavelength was kept at the desired value. Of the six targets irradiated for this experiment, the first three were produced from Li foil, and the second three were produced from Li bar.

Another set of six targets was irradiated, without the use of any cleaning shots, at a distance of 45 cm from the focusing lens. With one exception, each target was irradiated only once and each at a different power density than the others in an attempt to obtain visual evidence of unipolar arcing, and to establish the threshold power density at which arcing could occur. Due to a parts problem with the Sandia Laboratory SEM, the targets were transported to Monterey, California, to be observed by the SEM at NPS. One target was irradiated by several on-resonance pulses, and then by several off-resonance pulses at $\lambda = 666.4$ nm, in an attempt to obtain and compare plasma density data.

c. Experiment-Type 3

An additional set of six targets was transported to Monterey, California, a detailed surface analysis was done using an SEM, and about two dozen photographs of non-irradiated Li surfaces were taken. After moving them to a vacuum target chamber, five of the targets were irradiated by a CO_2 laser at NPS. For details on the

CO_2 laser, optics, and vacuum chamber setup see the thesis by Olson [Ref. 10: pp. 33-38]. One target was not irradiated in order to provide a control surface to determine which effects, if any, were caused by atmospheric exposure and which were caused by laser irradiation. One target was irradiated six times in an attempt to obtain plasma threshold power density information. The other four targets were each irradiated once and at a different power density than the other three, in order to obtain visual evidence of unipolar arcing and threshold power density information for arcing. The targets were again observed by the SEM, and about two dozen more photographs were obtained.

IV. EXPERIMENTAL RESULTS

A. TYPE 1 EXPERIMENTS

1. Lithium Targets

Obtaining visual evidence of unipolar arcing proved to be very difficult. Part of the problem was due to the rapid deterioration of the lithium surface upon exposure to air and water vapor. This led to, within two to three minutes, a dark grey layer of corrosion being formed over the entire surface, which was probably lithium nitride (Li_3N), a black nitride [Ref. 26: p. 15]. After several minutes of exposure to atmosphere a white powder, probably lithium oxide (Li_2O) or lithium hydroxide (LiOH) [Ref. 31: p. B-108], would form on the surface. The corrosion layers greatly affected the ability to distinguish arc craters from other surface details.

Another significant problem was the SEM used at SNLA. It was discovered, after several attempts to obtain good photographs, that the SEM had an oil contamination problem in the sample chamber, which on at least two occasions led to the further deterioration of the lithium target surfaces even while in the SEM under vacuum. Additionally, it was determined that the scintillation detector was malfunctioning, which adversely affected the contrast available for good photographs. This was discovered after a set of targets which had been looked at in the SEM at SNLA, were removed and transported to Monterey, California, and observed in the NPS SEM the next day. Instead of the expected further degradation due to exposure to atmosphere, the surfaces were much easier to see and several high quality photographs were taken.

At this point, it became apparent that non-irradiated Li surfaces had circular "nodules" which were similar in appearance to what the unipolar arc craters should look like. Figure 4.1 was obtained from a non-irradiated target, and white rimmed circular nodules of about 1 μm diameter can be seen. A target irradiated with seven shots at power densities which produced no noticeable plasma, and one plasma producing shot at 5.5 MW/cm^2 is shown in Figure 4.2. What appear to be unipolar arc craters are visible, but they are about the same size as the circular nodules in the previous figure on non-irradiated Li. Photographs taken of later batches of targets confirmed that the circular nodules were common to non-irradiated Li surfaces which were prepared as described in the last chapter, such as the one seen in Figure 4.3.

Figure 4.1 Non-Irradiated Li Surface at 1.6KX.

Figure 4.2 Irradiated Li Surface at 16KX.

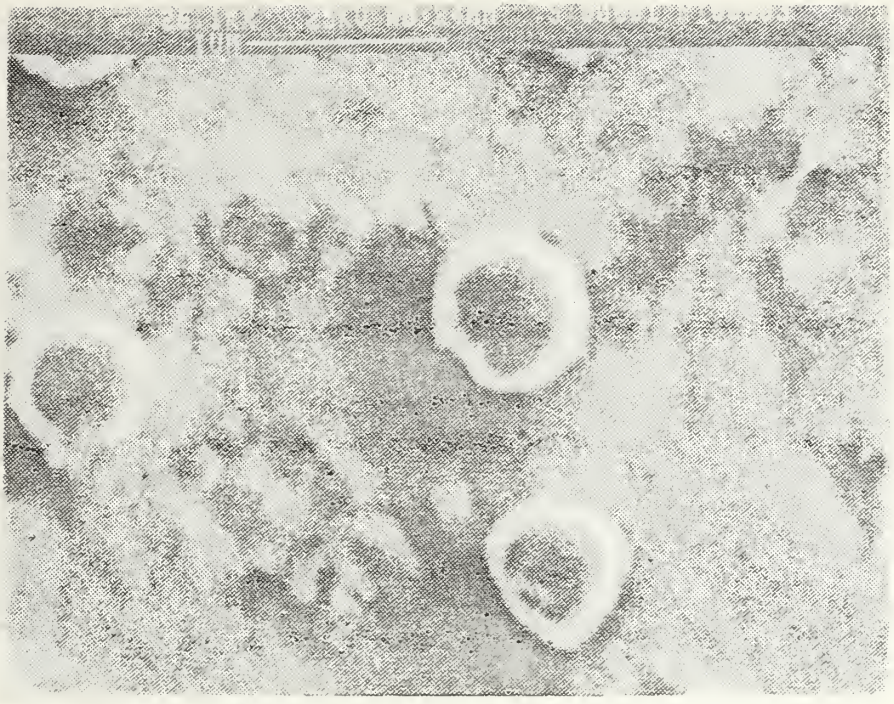

Figure 4.3 Circular Nodules on Non-Irradiated Li.

Additional comparisons between non-irradiated and irradiated surfaces are presented in Figures 4.4 and 4.5, both of which are of comparible magnification. Clearly visible in Figure 4.4 are numerous circular nodules, which appear to be protruding up out of the surface. This distinguishes them from the arc craters in Figure 4.5, whose centers appear to be "cupped" into and slightly below the surface, although the white crater rims may rise above the surface. These comparisons between nodules and craters, along with similar comparisons at different magnifications in several other photographs, lead to the possibility that the existing circular nodules, when irradiated, serve as starting points at which unipolar arcing can occur.

Figure 4.6 is of a target which had been subjected to eight plasma-producing shots ranging in power densities from 6.1-7.7 MW/cm^2. Initially, it was not believed that unipolar arc craters were present, but a series of photographs depicting similar looking craters from type 3 experiments provided strong evidence that arc craters were present in Figure 4.6. What apparently was happening was since Li had such a low melting point, about 181°C, the newly formed craters were filling back in with molten Li prior to re-solidification. The result was a kind of cupping effect, described earlier, as if a scoop of metal had been removed from the surface. This phenomena was not observed on any surfaces of non-irradiated Li.

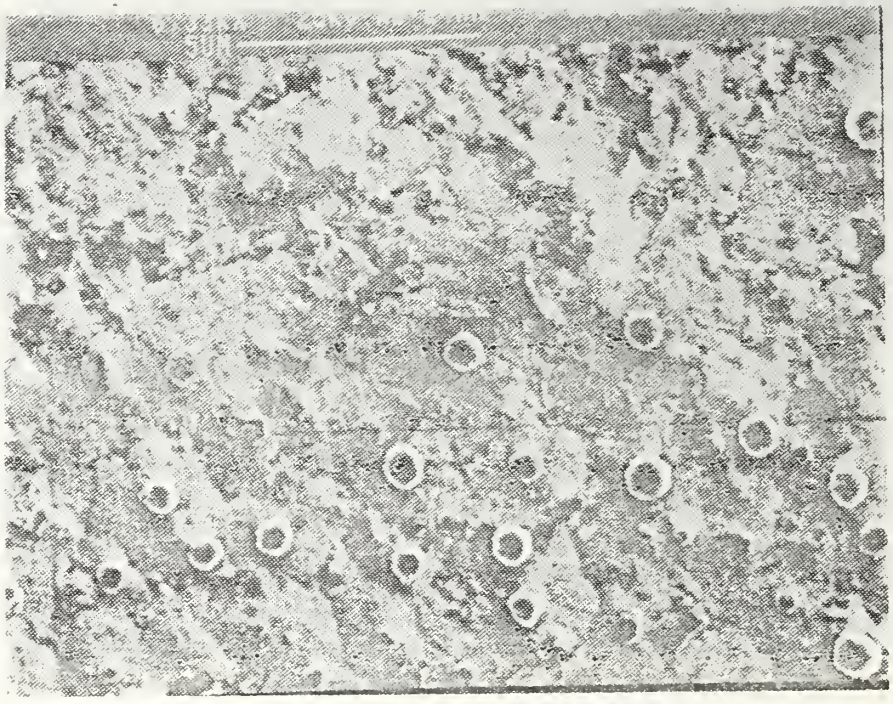

Figure 4.4 Circular Nodules on Non-Irradiated Li.

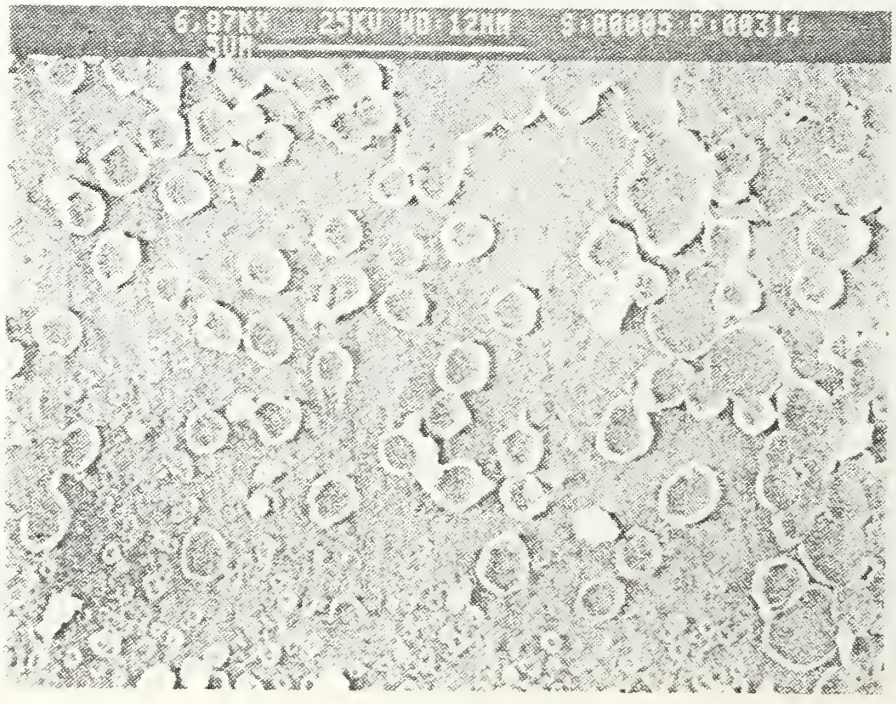

Figure 4.5 Arc Craters on Irradiated Li.

Figure 4.6 Irradiated Li Surface at 3.1KX.

Evidence of melting is shown in Figure 4.7 which was taken to the right of a focused laser impact crater. The photograph as shown, turned CCW by 90°, reveals a melted Li surface which traveled away from the laser impact crater and re-solidified as it cooled. The target was irradiated by eight plasma-producing laser pulses, ranging in power densities from 6.9-7.3 MW/cm^2. An example laser impact crater, taken from a single focused shot at 9.4 MW/cm^2, is shown in Figure 4.8 which depicts numerous molten droplets of Li which had been ejected from the crater. Due to problems with the SEM and the handling of Li, the threshold laser power density required to melt Li was not able to be determined.

2. **Stainless Steel Targets**

Three type 316 SS targets were irradiated by a dye laser with $\lambda = 670.8$ nm and pulse width (τ) = 800 ns. The first target was irradiated by a focused (f = 50 cm) pulse at a power density of 4.1 MW/cm^2. Bright plasma light was observed, and several pictures of unipolar arcs were obtained. Figure 4.9 was taken to the left of the laser impact crater, and three well-developed unipolar arc craters are clearly visible. The largest crater was about 10 μm in diameter, and the smallest was about 3 μm in diameter.

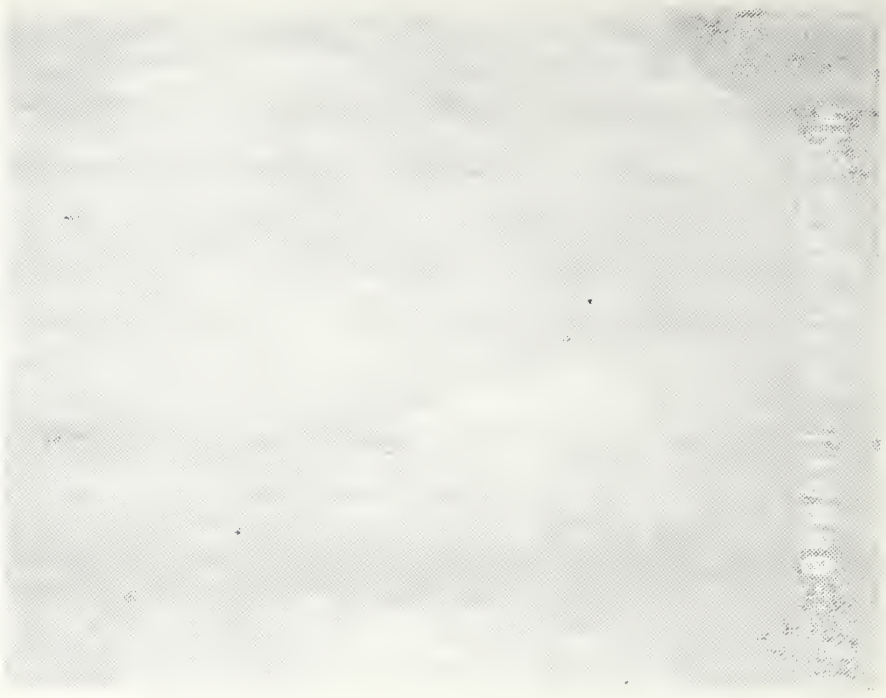

Figure 4.7 Laser Induced Melting on Li Surface.

Figure 4.8 Focused Laser Pulse on Li at 9.4 MW/cm^2.

Figure 4.9 Unipolar Arcs on 316 SS at 2.0KX.

Near the top of the photo, which was rotated CCW 90°, can be seen several "cupped" out craters, similar to those observed on lithium targets. Since they are located between the edge of the rim of the laser impact crater and the three unipolar arc craters, it is possible that they were newly formed arc craters that were filled in with molten steel prior to re-solidification. Why there were so many, and why they were not found elsewhere further from nor inside the laser impact area was not known. Unipolar arc craters were observed, in widely varying number densities (craters area), on out to the edge of the polished target surface. The laser impact crater, shown in Figure 4.10, was measured at about 0.87 mm in diameter, and shows evidence of melting throughout the impact area.

The second target was placed at 49 cm from the focusing lens and, when irradiated at 3.6 MW/cm^2, did not emit visible plasma light. No arc craters were found upon observation by an SEM. The third target, positioned 49.5 cm from the lens, was irradiated at a power density of 3.8 MW/cm^2. Plasma light was observed, and thus the threshold for plasma production was established at between 3.6 and 3.8 MW/cm^2 on 316 SS. The surface was observed briefly by an SEM, but neither the laser impact crater, which was clearly visible macroscopically, nor any evidence of unipolar arc

Figure 4.10 Laser Impact Crater Area on 316 SS at 100 X.

craters were found. This was attributed to a malfunctioning part on the SEM which made it very difficult to observe surface detail much smaller than 1-2 μm.

B. TYPE 2 EXPERIMENTS

Several sets of this type experiment were conducted in order to determine the best setup with regard to the equipment required, how the equipment was to be electrically and/or mechanically connected, and the most efficient procedure for data collection and recording. The data recorded included those necessary for power density calculations, such as FWHM laser spot diameter and energy on target, and for plasma density calculations. The FWHM pulse width was measured to be 840 ns, and λ was 670.8 nm for all but one set of data. The malfunctioning SEM part had not yet been replaced, and thus during the first set of experiments no attempts to observe Li surfaces were made.

After all laser shots were taken and the plasma data stored on disk, each data file was plotted by the computer. Unfortunately, it was not until this point that a bad data file would be discovered. Problems in data collection occurred when excessive plasma light intensity would saturate the OMA detector, thereby causing the plasma data to be

invalid for that particular shot. This happened with power densities ranging from 2.63-4.63 MW/cm^2 on various targets, but some pulses at power densities in excess of 5 MW/cm^2 on four of the six targets caused no saturation of the OMA detector, and thus the cause for periodic saturation is not known. At the low power density range (< 0.6 MW/cm^2), although the characteristic violet plasma light was often observed, the recorded plasma data would often be lost in the background noise.

A set of typical photographs of plasma line broadening are presented in the order of decreasing laser power density. The irradiated target was made from Li bar, and upon the first pulse at 4.77 MW/cm^2, the detector was saturated. On the next pulse, at 5.05 MW/cm^2, plasma data were satisfactorily recorded, and a density of about $9.8 \times 10^{16}/cm^3$ was calculated. Figure 4.11 depicts this, and it can be observed that the broadening is not symmetric. This large degree of assymmetry was noticeable only in the higher plasma density ($> 6 \times 10^{16}/cm^3$) levels and the reason for it is not known. All plasma density calculations are from actual FWHM measurements, and the maximum error, if the assymmetric portion should not be included, is $\leq 15\%$. The plasma density from Figure 4.12 was calculated to be $5.0 \times 10^{16}/cm^3$, and the laser power density was 2.13 MW/cm^2. The pulse is much narrower and more symmetric. The lowest relative intensity (vertical axis) value where the curve becomes nearly horizontal is where the baseline is obtained for plasma density calculations. As in the previous figure, interpolation is required to establish where the baseline is, due to the difference in relative intensities on the left and right hand sides of the photograph, and because the curve still has noticeable slope at the edges of the photograph.

The next three figures, for which the laser power densities were 1.18, 0.649, and 0.495 MW/cm^2 respectively, reveal steadily decreasing amounts of line broadening. In corresponding order, the plasma density in Figure 4.13 is $2.8 \times 10^{16}/cm^3$, and the shape is almost completely symmetric. The plasma density in Figure 4.14 is $1.3 \times 10^{16}/cm^3$, and the relative intensity has decreased significantly from that in Figure 4.11, such that the background noise is becoming very noticeable. Although all photographs were taken after the "zero" had been subtracted from the data, eventually plasma density decreased enough to become completely lost in the noise, as shown in Figure 4.15. Obviously, in this last figure, no value for plasma density can be obtained.

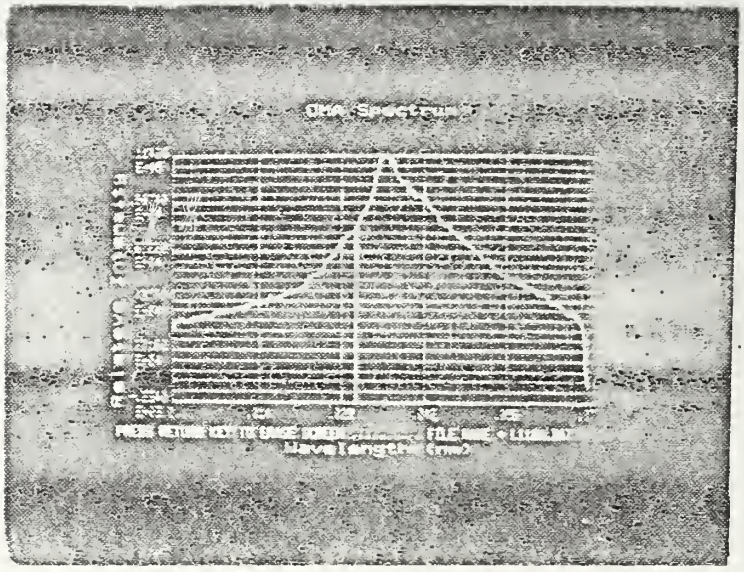

Figure 4.11 Plasma Broadening for Laser Power Density of 5.05 MW cm^2.

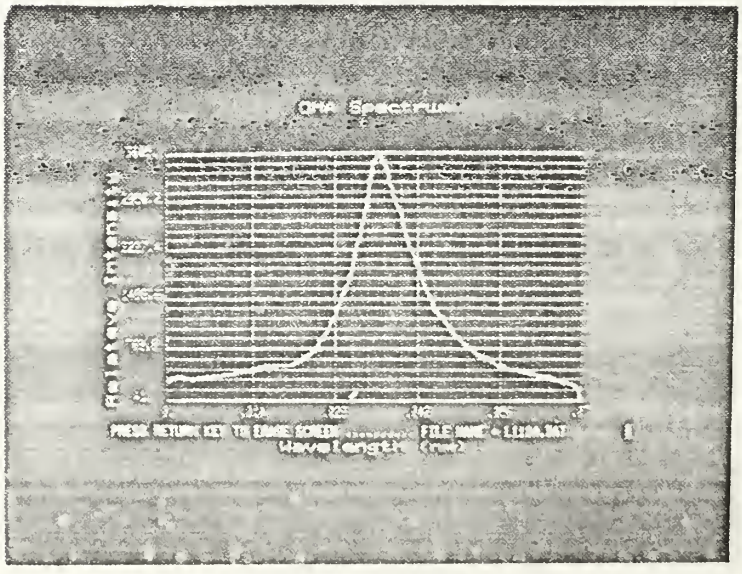

Figure 4.12 Plasma Broadening for Power Density of 2.13 MW cm^2.

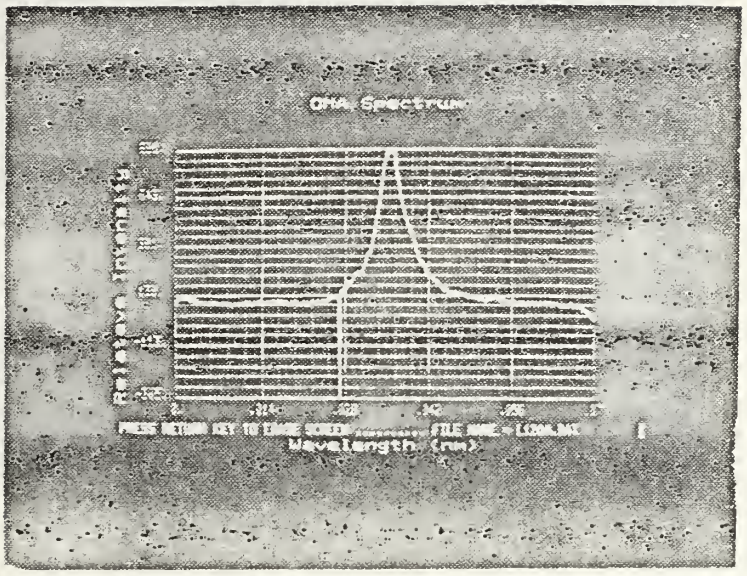

Figure 4.13 Plasma Broadening at 1.18 MW/cm^2.

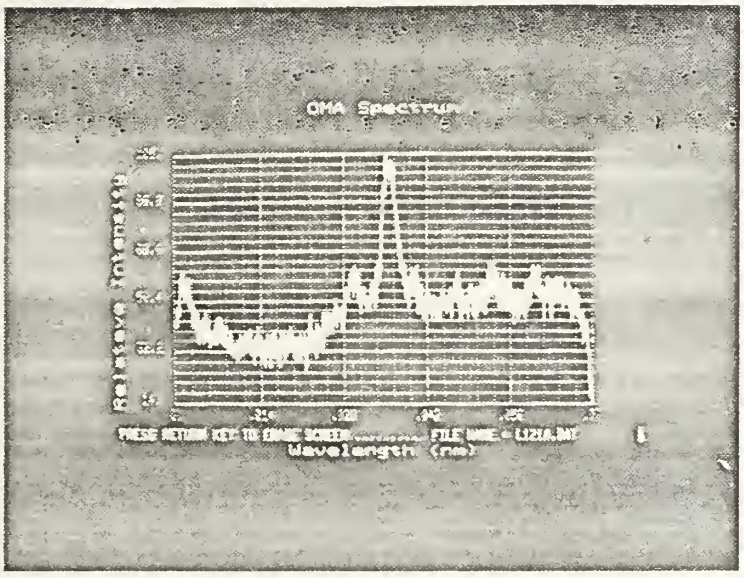

Figure 4.14 Plasma Broadening at 0.649 MW/cm^2.

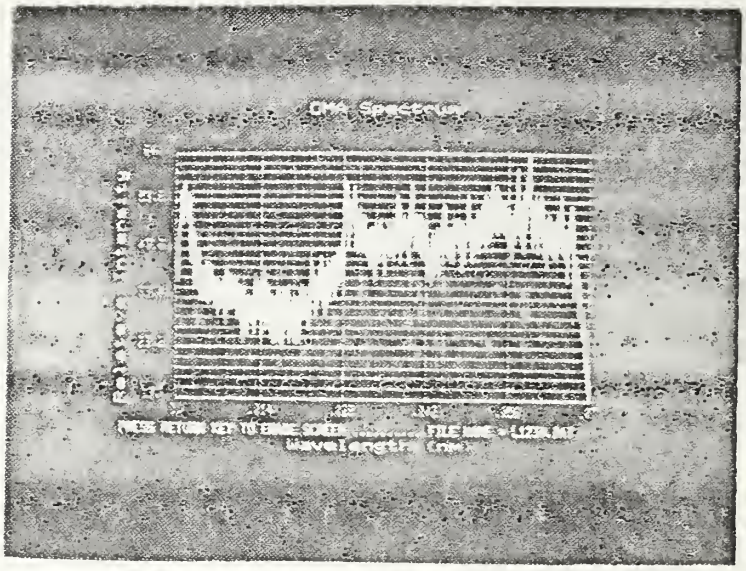

Figure 4.15 No Observable Plasma Broadening at 0.495 MW cm^2.

For the second and third Li foil targets irradiated in this experiment, the plasma densities produced are plotted against the corresponding laser power densities in Figure 4.16. Spot size data for the first target were recorded on photographs instead of being read from the reticon digitizer. Subsequently, the measurements were difficult and subjective, and thus imprecise and inaccurate in comparison with like data obtained on the other two targets. A similar graph for three Li bar targets is found in Figure 4.17. A roughly linear relationship can be observed between power density and plasma density for all targets.

Plasma densities for the bar targets were about 100% greater than those for the foil targets when irradiated at the higher power densities. Also, the slope of the data points for bar targets was steeper than that for the foil targets. Perhaps, due to more impurities contained in the foil targets, less quantities of Li neutrals were available for ionization. The threshold power density required for detectable (by OMA) plasma broadening was $\sim$ 0.5 MW/cm^2 for both bar and foil targets.

Data from the experiment conducted on bar Li using on- and off-resonance laser pulses is plotted in Figure 4.18. Unfortunately, the results were inconclusive and misleading. The plasma density values obtained during on-resonance pulses were much less than anticipated. This was most likely due to poor laser dye performance after a

Figure 4.16 Power Density vs Plasma Density
for Li Targets made from Foil.

Figure 4.17 Power Density vs Plasma Density
for Li Targets made from Bar.

few hundred shots had been taken on it. Laser burn spots on exposed polaroid film paper verified that the laser pulses were weak and non-uniform. The laser was then re-tuned to $\lambda = 666.4$ nm, which was closer to the peak of the effective range of the dye mix. Laser output energy immediately increased by about 20%. New burn patterns on film indicated that the laser pulses were significantly improved, both in overall power and in uniformity. Thus, the power density for off-resonance pulses was increased, and the result was higher plasma density measurements, but only for the unattenuated pulses. No Li 460.3 plasma information was obtained on any of the off-resonance attenuated pulses, all of which were at power densities of < 4 MW/cm^2. Instead, a weak but distinct and slightly broadened plasma pulse was recorded at a wavelength of 466.4 nm for all attenuated off-resonance pulses. The source for this plasma line was not determined. Due to time and equipment availability constraints, no additional on/off resonance experiments were conducted.

Another disappointing aspect of this thesis concerned the second set of six Li targets which were irradiated as previously described and transported to NPS for visual inspection by an SEM. Despite hours of detailed observations, no visual evidence of unipolar arcing on any target could be found, although plasma density data were recorded by the OMA. The most plausible reason was that existing surface corrosion or contaminants were not removed from the targets since cleaning shots were not taken. However, cleaning shots would have altered the surface and thus would have invalidated the desired data for arcing threshold power density measurements. Another reason may be that inadvertant exposure to air and water vapor may have caused the surfaces to become so obscured that no arc craters were visible. This actually happened on the set of targets which will be reported in the type three experiment section.

After a new dye change, plasma profiles were photographed. Figure 4.19 is a profile, through the lucite window of the vacuum chamber, of the target holder. A plasma pulse produced from an on-resonance laser pulse of about 200 milli-joules (mJ) is presented in Figure 4.20. Unfortunately, due to time constraints, laser power density measurements were not obtained. Also, due to repositioning the fiber optic to make room for the camera, no plasma density information was collected. The extent of the plasma from the target is about 3 mm.

Figure 4.18 Plasma Density vs Power Density
for On/Off Resonance Laser Pulses.

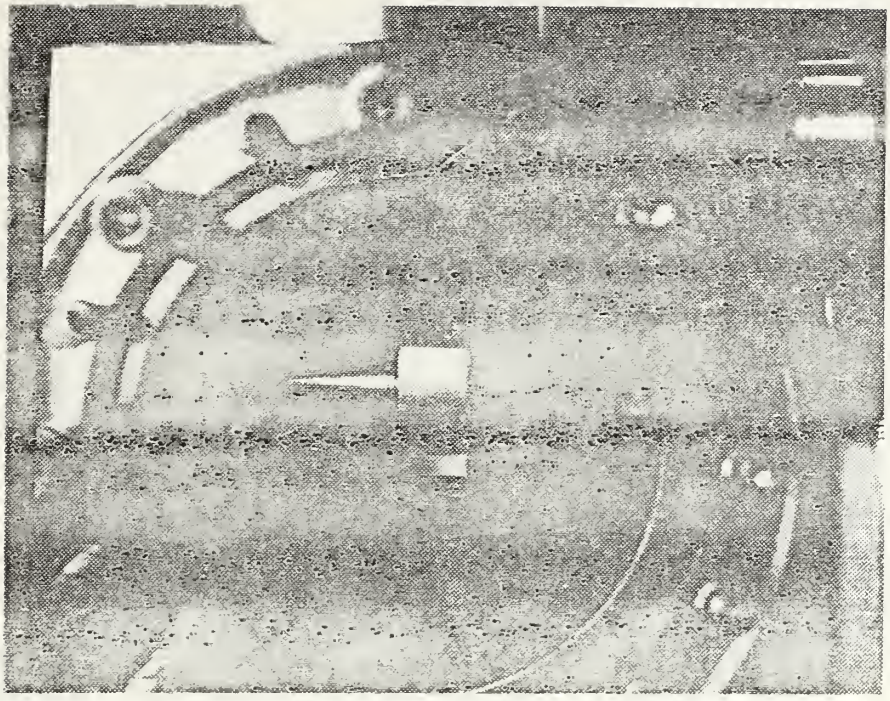

Figure 4.19 Profile of Target Holder in Vacuum Chamber.

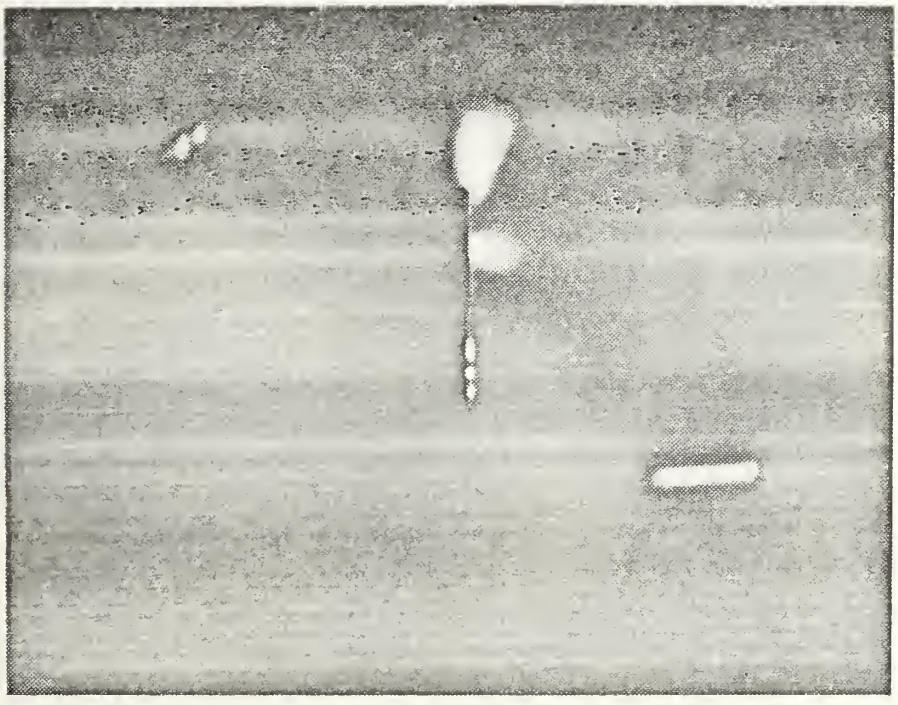

Figure 4.20 Profile of Li Plasma Light.

C. TYPE 3 EXPERIMENTS

Six Li targets surfaces were thoroughly inspected by an SEM, and five of the six targets were irradiated by a CO_2 laser at $\lambda = 10.6$ μm and $\tau = 4.55$ μsec. Positive evidence of unipolar arcing was obtained upon post-irradiation inspection of the surfaces. Examples of circular nodules, which were present on all six non-irradiated targets, are shown in Figure 4.21. At about the same magnification, striking evidence of unipolar arcing is shown in Figure 4.22, which was taken on target three, irradiated at 0.091 MW cm^{-2}. Numerous craters are visible, which have a similarly cupped appearance as those found previously in the type one experiments. Several other photographs depicting multiple cratering, as in Figure 4.22, were obtained. Another example of multiple craters, found on the same target as above, is shown in Figure 4.23, where it appears that the large crater on the left was expanding and overtaking the smaller craters around it.

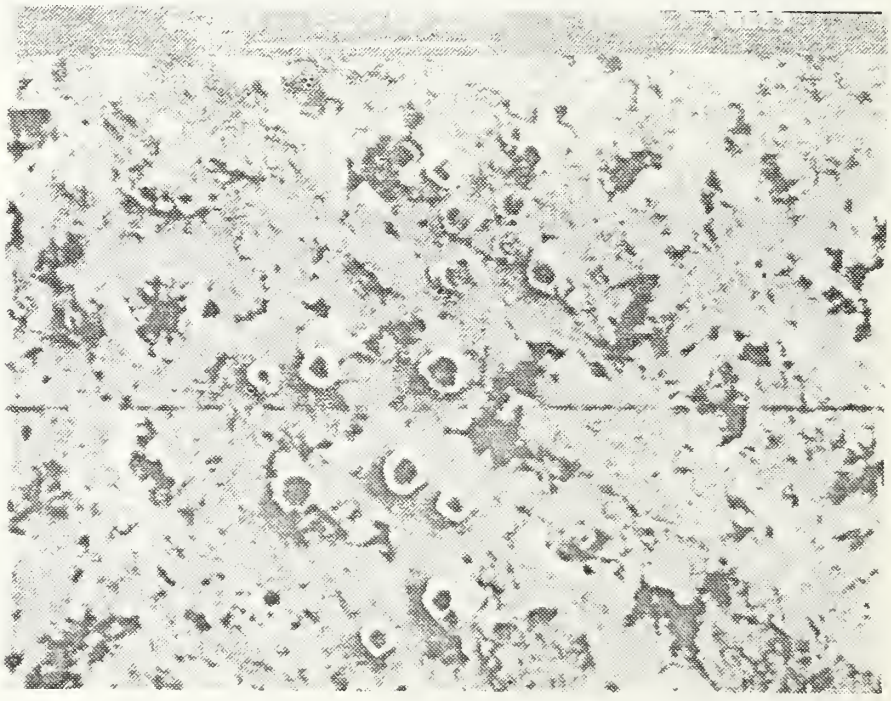

Figure 4.21 Circular Nodules on Non-Irradiated Li.

Due to a burned out filament in the NPS SEM, the irradiated Li targets had to be removed and placed in a sealed, nitrogen filled jar. Upon resuming surface observations, it was readily apparent that surface degradation had occurred in the short

Figure 4.22 Multiple Arc Craters at
Power Density of 0.091 MW/cm^2.

time the samples were exposed to air and water vapor. This made surface details very hard to see, which required even more time to carefully look at the surface. Unipolar arcs were still visible, although very difficult to see, on target five, which was irradiated at 0.062 MW/cm^2. This was the lowest power density of any data reported in this thesis at which visible plasma was produced and arc craters, seen in Figure 4.24, were visible. The cupped unipolar arc craters were observed only on laser irradiated Li surfaces, and were not found on any other Li surfaces which were not irradiated.

D. STATISTICAL AND ERROR ANALYSIS

Measurement errors can fall into three main groups--mistakes, systematic errors, and random errors. Mistakes, which include arithmetic and counting type errors, were reduced to a minimum by the process of repeating all calculations which were reported in this thesis. If a difference was obtained between the first and second calculation, it was repeated until the satisfaction of a correct result was assured. Mistakes made by the misreading of instruments or incorrectly recording data were hopefully kept to a minimum based on the author's attention to detail and data gathering experience. The magnitude of statistical errors depends on the accuracies of equipment used and of the

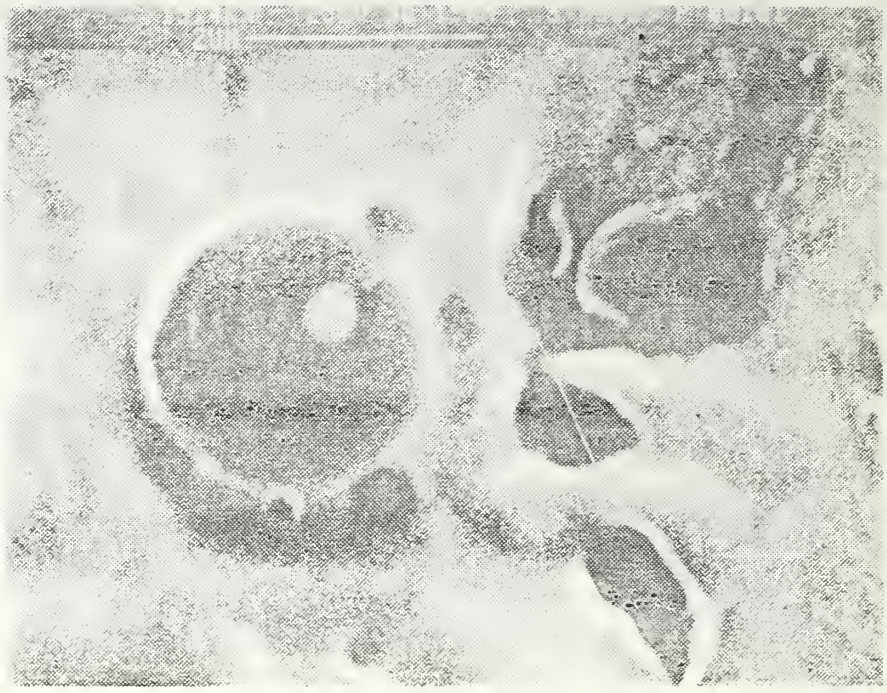

Figure 4.23 Multiple Arc Craters on Li Surface.

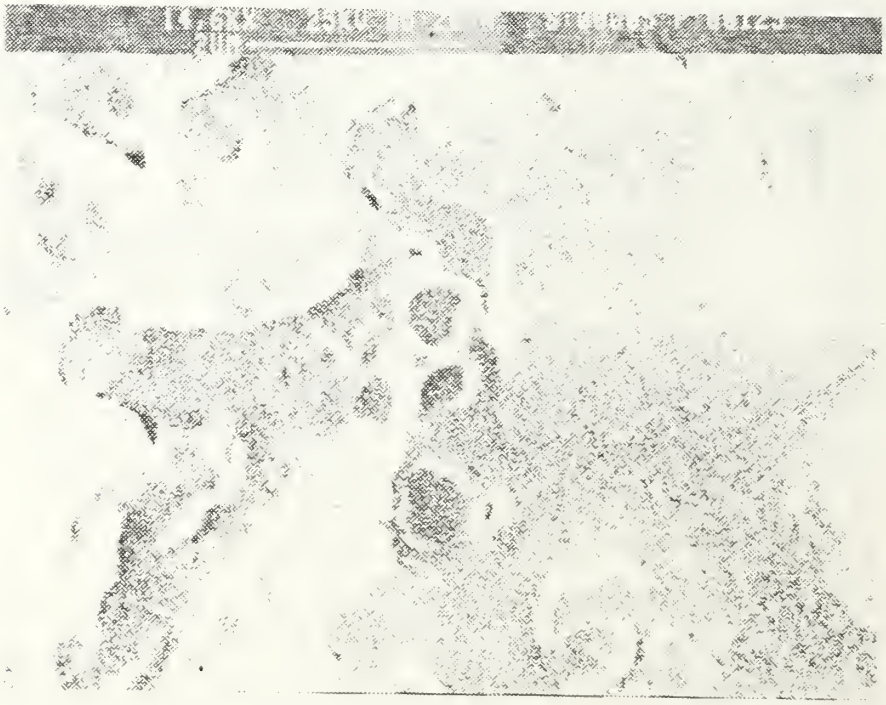

Figure 4.24 Arc Craters at Threshold Power Density.

values obtained from references on such data as the mass of an electron. The author is confident of the accuracy of all equipment used based on the experience of the personnel who operated and maintained the equipment on a periodic basis, and on calibration data as applicable. However, the method one uses to take measurements is always capable of introducing systematic error, and thus the experience of the author is again relied upon as well as occasionally having an observed value confirmed by another person.

Random errors result, for example, from the differences between an average of many data and an individual datum. Since these errors are of a statistical nature, they can be dealt with statistically. For example, all measurements taken to establish an average value were compared to a range which was twice the standard deviation (σ) from below or above the average value itself. Any datum outside 2σ from the average was discarded. In other words, data within 2σ from the average was considered to have a 95% probability of being statistically valid.

The estimation of errors in quantities that were functionally related, such as power density measurements, was treated in the standardly accepted manner [Ref. 33]. Thus, the error in power density measurements, taking into account the measurement errors for FWHM spot diameter, τ, and energy meter readings as well as ratios, was estimated to be 3%. For plasma density measurements, the estimated error was 5%, based on calculational uncertainties only. From a review of experimental vs theoretical predictions, the error approaches 50% [Ref. 32: p. 240].

V. SUMMARY

A. CONCLUSIONS

1. Unipolar Arcing Studies

Several lithium targets were irradiated by a dye laser tuned to the first resonance line of Li, at 670.8 nm, and by a CO_2 laser at $\lambda = 10.6$ μm. Evidence of unipolar arcing was found on targets irradiated at both wavelengths, although most of the arc craters observed did not display the deep central crater and pronounced rim of the model arc crater appearance. The craters observed on Li had a cupped or scooped out appearance, which was possibly due to molten Li flowing back into and filling the center of the arc crater. Another possibility is that, due to the softness and low melting temperature of Li, the arc craters may have expanded laterally from the center instead of vertically into the metal. The reasons postulated above will only be verified upon a detailed analysis of plasma-Li surface interactions in a closely controlled environment so as to prevent any external disturbance of the Li surface before, during, and after irradiation by a laser.

The threshold power density for unipolar arcing on lithium was determined to be, based on data obtained only from CO_2 laser irradiation experiments, less than about 0.06 MW/cm^2. Arc craters were not observed on any Li targets irradiated by the dye laser with a single pulse, thus the threshold power density could not be established for unipolar arcing caused from on-resonance wavelength pulses. The reason for this was thought to be that, due to the extremely reactive nature of Li, any arc craters on the surface were quickly obscured upon exposure to air and water vapor. Although exposure was kept to a minimum at all times, the Li targets irradiated at the on-resonance wavelength specifically for the purpose of determining the unipolar arcing threshold had to be transported to the NPS SEM in Monterey, California for observation. This resulted in a delay of > 24 hours and additional target transfer operations, which required additional exposure to the atmosphere.

Unipolar arcing was clearly observed on type 316 SS targets, which were irradiated by the dye laser at $\lambda = 670.8$ nm. The threshold laser power density for unipolar arcing was coincident for that required for plasma formation, which was ≤ 4.1 MW/cm^2.

2. Plasma Density Analysis

The threshold laser power density for on-resonance wavelength pulses, required to produce a detectable plasma density (by OMA) from Li targets, was about 0.5 MW/cm^2.The corresponding plasma density was $< 2 \times 10^{16}/cm^3$. For laser power densities between 2.5-5.0 MW/cm^2, the plasma densities produced from Li bar targets, which ranged from ≤ 6 to $\geq 10 \times 10^{16}/cm^3$, were about twice those produced from Li foil targets. This was possibly the result of large numbers of impurities in the Li foil interfering with the efficient ionization of Li neutrals. Thus, Li plasma densities that meet ion source requirements for PBFA II were observed at the higher laser power densities used in these experiments.

Comparisons between lithium plasma densities produced from on- and off-resonance pulses were inconclusive due to an insufficient amount of data collected and because the laser pulse intensity was markedly more uniform when the laser was re-tuned to the off-resonance wavelength of 666.4 nm. This was because the lower wavelength was closer to the peak efficiency range for the dye mix used. Thus, the theorized improvement in plasma production due to the proposed combination of LIBORS and unipolar arcing could not be verified.

B. RECOMMENDATIONS

The most advantageous improvement for the experiments conducted in this thesis would have been a strictly controlled environment for the entire Li experiment cycle, including production of targets, pre- and post-observation in the SEM, and irradiation by a laser while under vacuum. Other improvements would include the method of Li target production, and equipment usage and diagnostics. Also, a strong recommendation for possibly improving the plasma density obtained for a given laser power density would be to irradiate Li targets at elevated temperatures below the melting point, for example between 150°-170°C. This could result in the more rapid release of neutrals from the solid surface with a subsequent increase in ionizations and plasma density.

Various methods should be investigated to improve the Li target's ability to withstand exposure to atmosphere. For example, vacuum deposited Li in thin layers could be coated with a thin ($\sim 1\mu m$) layer of a non-reactive alloy of Li, or some other suitable coating, which could withstand exposure and still protect the pure Li underneath. A more suitable substrate, such as niobium, tantalum, or molybdenum as

previously recommended in this thesis, that will not adversely react with Li, as did the SS, nor act as a catalyst and affect experimental results, should be developed and investigated.

The OMA equipment setup should have been better optimized for improved plasma density studies. One major improvement would have been to decrease the detector gate open time to the specific interval required to detect only the desired Li 460.3 nm line broadening, and thus all adverse sources of noise would have been greatly reduced. This was a limitation in detecting and calculating the threshold plasma densities produced at low laser power densities. Another recommendation is to determine the reason for occasional detector saturation, which caused plasma data to be lost during several high laser power density pulses.

Finally, a conclusive investigation of plasma density and laser power density studies for on- and off-resonance wavelength pulses on Li should be conducted. This would possibly provide conclusive evidence regarding plasma production improvement theorized by the combination of the LIBORS and unipolar arc processes. Such a study could include using pulsed dye lasers at different wavelengths to determine time relationships of the plasma production process as an aid to characterize both the unipolar arc and LIBORS processes, individually and together.

LIST OF REFERENCES

1. VanDevender, J.P., and Cook, D.L., "Inertial Confinement Fusion with Light Ion Beams," *SCIENCE*, v. 232, pp. 831-836, 16 May 1986.

2. Pregenzer, A.L., "Electrohydrodynamically driven large-area liquid-metal ion sources," *Journal of Applied Physics*, v. 58(12), pp. 4509-4511, 15 December 1985.

3. Cook, D.L., and others, *Progress in Light Ion Beam Fusion Research on PBFA II*, paper presented at the 13th Institute of Physics Conference on Plasma Physics, Oxford University, England, 2-4 July 1986.

4. Gerber, R.A., and others, "Light Ion Sources for ICF," *IEEE Transactions on Nuclear Science*, v. NS-32(5), pp. 1718-1722, October 1985.

5. Schwirzke, F., *Unipolar Arcing, A Basic Laser Damage Mechanism*, paper presented at the Fourteenth Annual Symposium on Optical Materials for High Power Lasers, National Bureau of Standards, Boulder, Colorado, 16-17 November 1982.

6. Keville, M.T., and Lautrop, R.W., *An Investigation of Unipolar Arcing Damage on Stainless Steel and Titanium Carbide Coated Surfaces*, M.S. Thesis, Naval Postgraduate School, Monterey, California, June 1980.

7. Ryan, F.T., and Shedd, S.T., *A Study of the Unipolar Arcing Damage Mechanism of Selected Conductors and Semiconductors*, M.S. Thesis, Naval Postgraduate School, Monterey, California, June 1981.

8. Goodall, D.H.J., and others, "Investigations of Arcing in the DITE Tokamak," *Journal of Nuclear Materials*, v. 76-77, pp. 492-498, 1978.

9. Dreike, P.L., and Tisone, G.C., "Production and diagnosis of a lithium anode plasma source for intense ion beam diodes," *Journal of Applied Physics*, v. 59(2), pp. 371-377, 15 January 1986.

10. Olson, J.S., *CO_2 Pulsed Laser Damage Mechanisms and Assessment of Plasma* Effects (Unfocused Beam), M.S. Thesis, Naval Postgraduate School, Monterey, California, December 1986.

11. Naval Postgraduate School Report NPS-61-82-002, *Basic Mechanisms that Lead to Laser Target Damage*, by F. Schwirzke, M.H. Beelby, and H.G. Ulrich, 5 October 1981.

12. Schwirzke, F., and Taylor, R.J., "Surface Damage by Sheath Effects and Unipolar Arcs," *Journal of Nuclear Materials*, v. 93 and 94, pp. 780-784, 1980.

13. Halbritter, J., "Dynamical Enhanced Electron Emission and Discharges at Contaminated Surfaces," *Applied Physics A*, v. 39, pp. 49-57, 1986.

14. Air Force Weapons Laboratory Report AFWL-TR-73-92, *Explosive Electron Emission and the Characteristics of High-Current Electron Flow*, by R. K. Parker, pp. 17-18, February 1974.

15. Naval Postgraduate School Report NPS-61-84-004, *Short Pulse Laser and Plasma Surface Interactions*, by F. Schwirzke, 2 April 1984.

16. Hudson, R.D., and Carter, V.L., "Atomic Absorption Cross Section of Lithium Vapor Between 2300 and 1150 Å," *Physical Review*, v. 137(6A), pp. 1648-1650, 15 March 1965.

17. Measures, R.M., "Electron Density and Temperature Elevation of a Potassium Seeded Plasma by Laser Resonance Pumping," *Journal of Quantitative Spectroscopy and Radiative Transfer*, v. 10(1), pp. 107-125, 1970.

18. McIlrath, T.J., and Lucatorto, T.B., "Laser Excitation and Ionization in a Dense Li Vapor: Observation of the Even-Parity, Core-Excited Autoionizing States," *Physical Review Letters*, v. 38(24), pp. 1390-1393, 13 June 1977.

19. Measures, R.M., "Efficient Laser Ionization of Sodium Vapor - A Possible Explanation based on Superelastic Collisions and Reduced Ionization Potential," *Journal of Applied Physics*, v. 48(7), pp. 2673-2675, July 1977.

20. Measures, R.M., and Cardinal, P.G., "Laser Ionization Based on Resonance Saturation - a Simple Model Description," *Physical Review A*, v. 23(2), pp. 804-815, February 1981.

21. Lindgard, A., and Nielsen, S.E., "Transition Probabilities for the Alkali Isoelectronic Sequences Li I, Na I, K I, Rb I, Cs I, Fr I," *Atomic Data and Nuclear Data Tables*, v. 19(2), pp. 533-633, 1977.

22. Candela Corporation, *Instructions for SLL Dye Laser Systems*, Revision A, June 1977.

23. EG&G Princeton Applied Research Technical Note 181, *Gated Operation of OMA-2 Detectors*, June 1981.

24. EG&G Princeton Applied Research, *Model 1420 Solid State Detector Operation and Service Manual*, February 1980.

25. EG&G Princeton Applied Research, *Model 1211 Pulse Generator Operation and Service Manual*, August 1979.

26. Averill, W.A., and others,in *Proceedings of the First International Aluminum-Lithium Conference*, edited by Sanders, T.H., Jr., and Starke, E.A., Jr., (Stone Mountain, Georgia, 19-21 May 1980), pp. 9-28.

27. *Metals Handbook*, 9th ed., v. 2, pp. 762-763, American Society for Metals, 1979.

28. *Metals Handbook*, 8th ed., v. 1, p. 1213, American Society for Metals, 1961.

29. Bieg, K.W., Private communication, Sandia National Laboratory, Albuquerque, New Mexico, October 1986.

30. Griem, H., *Plasma Spectroscopy*, pp. 63-88, 454-456, McGraw-Hill, Inc., 1964.

31. *Handbook of Chemistry and Physics*, 56th ed., CRC Press, Inc., 1975.

32. Konjevic, N., and Roberts, J.R., "A Critical Review of the Stark Widths and Shifts of Spectral Lines from Non-Hydrogenic Atoms," *Journal of Physical and Chemical Reference Data*, v. 5(2), pp. 209-257, 1976.

33. Beers, Y., *Introduction to the Theory of Error*, pp. 1-35, Addison-Wesley Publishing Company, Inc., 1953.

INITIAL DISTRIBUTION LIST

		No. Copies
1.	Defense Technical Information Center Cameron Station Alexandria, Virginia 22304-6145	2
2.	Library, Code 0142 Naval Postgraduate School Monterey, California 93943-5002	2
3.	Professor F. R. Schwirzke, Code 61Sw Department of Physics Naval Postgraduate School Monterey, California 93943-5000	2
4.	Professor K. E. Woehler, Code 61Wh Department of Physics Naval Postgraduate School Monterey, California 93943-5000	1
5.	Department Chairman Department of Physics Naval Postgraduate School Monterey, California 93943-5000	1
6.	Plasma Physics and Laser Laboratory Spanagel Hall (Bldg. 232, Rm. 27) Naval Postgraduate School Monterey, California 93943-5000	2
7.	Lieutenant Bruce A. Hoselton 2305 Deanna N.E. Albuquerque, New Mexico 87112	2
8.	Doctor Robert A. Gerber Laser Projects Division 1244 Sandia National Laboratory P.O. Box 5800 Albuquerque, New Mexico 87185	5
9.	Commander John S. Olson SPC-30 Polaris Missile Facility Atlantic Charleston, South Carolina 29408-5700	1

221036

Thesis
H8075
c.1

Hoselton
Optical characteristics of lithium plasma produced by laser irradiation.